The Thesis Committee for Andrew James Smith
certifies that this is the approved version of the following thesis:

OBSERVATIONS AND MODELS OF VENTING AT DEEPWATER GULF OF MEXICO VENTS

APPROVED BY

SUPERVISING COMMITTEE:

Supervisor:

Peter B. Flemings

Patrick M. Fulton

Marc Hesse

Xiaoli Liu

OBSERVATIONS AND MODELS OF VENTING AT DEEPWATER GULF OF MEXICO VENTS

by

Andrew James Smith, B.A.

Thesis

Presented to the Faculty of the Graduate School of

The University of Texas at Austin

in Partial Fulfillment

of the Requirements

for the Degree of

Master of Science in Geological Sciences

The University of Texas at Austin

August 2012

Acknowledgements

I thank my parents for their steadfast love and for always encouraging me to pursue my dream of becoming a geoscientist. If I am successful in life, it will be due entirely to their guidance and support. I thank my older sister, Emmy, for being my best friend and for always being a phone call away to talk about my romantic interests, our next adventure, and very large snowballs. I also thank my younger siblings, Ellen and Warren, for all the front-yard soccer games, late-night phone calls (Ellen), and grumpy messages (Warren). Thanks for reminding me not to grow up too quickly.

I have benefited from having friendly, hard-working, and helpful officemates during my time at UT (Baiyuan, Michael, and Will). In particular, I want to acknowledge Michael Merrell for always working through software issues (GMT) and technical difficulties with me. I greatly appreciate all the technical help and guidance that I've received from Derek Sawyer and Yao You. I thank Tessa Green for administrative help and for always squeezing me into Peter's busy schedule. I am also grateful for the friendliness and helpfulness of the rest of the UT/MIT Geofluids team.

This thesis would not have been possible without the guidance of Xiaoli Liu, Patrick Fulton, and Peter Flemings. I am extremely fortunate to have been advised by such exceptional people who provided invaluable science discussions and tremendous support and encouragement throughout my past two years here. Xiaoli: thank you for all the technical, intellectual, and moral support with the third chapter. Patrick: if you can teach me about heat flow, you can teach anyone. Thanks for your patience and for always being available to discuss a paper or idea. Peter: I will miss the morning runs and the 4

AM emails. Thank you for believing in me from the start and for always pushing me to be a better scientist. You are an extraordinary advisor and researcher.

Finally, I am appreciative of financial support from the UT/MIT Geofluids Consortium (Schlumberger, BHP Billiton, ConocoPhillips, ExxonMobil, BP, Anadarko, Hess, Total, Shell, Statoil, and Chevron), the Jackson School Hilcorp and Nexen Fellowship, and the ConocoPhillips SPIRIT Scholarship.

Abstract

OBSERVATIONS AND MODELS OF VENTING AT DEEPWATER GULF OF MEXICO VENTS

Andrew James Smith, M.S.Geo.Sci.

The University of Texas at Austin, 2012

Supervisor: Peter B. Flemings

Natural vents in the Gulf of Mexico are actively expelling water and hydrocarbons. They are ubiquitous along continental margins, and I characterize a single vent in the Ursa Basin at leaseblocks MC852/853. Seismic data reveal that the vent is elevated ~75 meters above the seafloor and is roughly circular with a ~1.2 km diameter. A transparent zone centered underneath the vent extends to ~1500 meters below seafloor; this zone is commonly interpreted to record the presence of gas. There is a strong negative polarity seismic reflection that rises rapidly at the vent's boundaries and is horizontal within a few meters of the seafloor beneath the vent edifice. I interpret that this reflection records a negative impedance contrast, marking the boundary between hydrate and water above and free gas and water below: it is the bottom-simulating reflector. Salinities beneath the vent increase from seawater concentrations to >4x seawater salinity one meter below seafloor. Temperature gradients within the vent are ~15x the background geothermal gradient.

I model the coexistence of high salinity fluids, elevated temperature gradients, and an uplifted bottom-simulating reflector with two approaches. First, I assume that high

salinity fluids are generated by dissolution of salt bodies at depth and that these hot, saline fluids are expelled vertically. Second, I model the solidification of gas hydrate during upward flow of gas and water. In this model, free gas combines with water to form hydrate: salt is excluded and heat is released, resulting in the generation of a warm, saline brine. The two models result in predictable differences of salinity and temperature. A better understanding of the hydrogeological processes at vent zones is important for quantifying the fluxes of heat and mass from submarine vents and is important for understanding the conditions under which deep-sea biological vent communities exist.

Table of Contents

List of Tables

List of Figures

Chapter 1: INTRODUCTION

Natural seafloor vents are ubiquitous on the continental slope in the Gulf of Mexico (GoM) and are actively expelling water and hydrocarbons. Vents are the site of poorly understood chemosynthetic biological communities [*Paull et al.*, 1984] and gas hydrate [*Brooks et al.*, 1986], an ice-like crystalline compound that contains methane and other light gases in a lattice of water molecules [*Sloan*, 1998]. Vents and associated hydrates release considerable quantities of hydrocarbon into the ocean [*Suess et al.*, 1999; *Valentine et al.*, 2001] and atmosphere [*Solomon et al.*, 2009], which may contribute significantly to oceanic and atmospheric carbon budgets [*Dickens*, 2003; *Judd et al.*, 2002; *Kopf*, 2002; *Milkov et al.*, 2003].

In seismic data, vents look like volcanic edifices. They are elevated ~100 m relative to the surrounding seafloor, and their cores are circular and up to several kilometers in diameter. The bottom-simulating reflector (BSR), which is interpreted to mark the boundary between hydrate and water above and gas and water below [*Bangs et al.*, 1993], rises toward the seafloor at the center of vents [*Hornbach et al.*, 2005; *Spieß and Fekete*, 2011; *Wood et al.*, 2002]. Elevated salinities and high temperature gradients have been observed in the subsurface near the seafloor of vents [*Paull et al.*, 2005; *Ruppel et al.*, 2005]. Although the coexistence of high salinities, elevated temperature gradients, and an uplifted BSR has been well documented, the hydrogeological processes creating these conditions remain poorly understood.

Some studies have proposed that high salinities at vents result from the upward flow of solute-enriched fluids superimposed on vertical diffusive solute transport [*Hanor*

and Mercer, 2010; *McManus and Hanor*, 1993]. Others have shown that high salinities can be generated via the exclusion of salt during hydrate formation [*Liu and Flemings*, 2006] or by subcritical phase separation [*Reitz et al.*, 2007]. To explain elevated temperature gradients, studies [e.g. *Hornbach et al.*, 2005] have applied an analytical solution to the steady-state advection-diffusion heat equation [*Bredehoeft and Papaopulos*, 1965], suggesting that the upward flow of warm fluids is elevating temperatures near the seafloor. Others have proposed that that the conductive effects of an underlying salt body may explain temperature anomalies [*Hornbach et al.*, 2005]. A separate study that uses a coupled model of fluid-heat-salt transport shows how salt-body geometry and seafloor relief may spur salt-driven geothermal convection on a regional scale [*Wilson and Ruppel*, 2007]. Finally, the release of heat during hydrate crystallization has been proposed as a significant heat-generating mechanism at vents [*Liu and Flemings*, 2006]. Although several processes have been recognized that may contribute to increases in salinity and temperature gradients, a dominant process that can fully explain both observations has yet to be described.

Another persistent issue related to vents is quantifying the flux of water and hydrocarbons. Several studies have estimated water flux by simulating measured subsurface geochemical profiles or temperature anomalies with advection-diffusion models [*Hornbach et al.*, 2005; *Reitz et al.*, 2007; *Ruppel et al.*, 2005], but these models have all assumed single-phase flow of water despite substantial evidence of multiphase flow such as: direct observations of active gas and oil venting [*Hornbach et al.*, 2005; *MacDonald et al.*, 2003; *MacDonald et al.*, 2000], sea surface slicks observed from space [*Macdonald et al.*, 1993], and the retrieval of oil-stained cores and highly gas-charged sediment from vent surfaces [*Ruppel et al.*, 2005; *Winters et al.*, 2007]. Several studies

have used video-imaging techniques [*Leifer and Macdonald*, 2003], sonar data [*Hornafius et al.*, 1999], or turbine tents on the seafloor [*Leifer and Boles*, 2005] to quantify the emission of hydrocarbons from individual vents. These techniques, however, do not constrain fluxes of both water and hydrocarbons, and they do not measure flow over long timescales. Furthermore, video-imaging techniques and turbine tents can only quantify flux at localized seep points and therefore are not effective for vents commonly found on continental slopes. The fluxes of gas and water need to be constrained in order to predict the relative role of hydrate formation in elevating salinity and temperature at vents [*Liu and Flemings*, 2007; *Xu and Ruppel*, 1999]. Thus, a universal method for estimating fluid flux is important for better understanding the hydrogeological process of venting. A method for estimating fluid flux from vents is also needed to constrain vents' global input of heat, mass, and carbon.

My thesis focuses on a seafloor vent in the GoM at leaseblocks MC852/853 in ~1070 meters of water depth. The vent has been studied extensively. Sediments are highly gas charged [*MacDonald et al.*, 2003; *Winters et al.*, 2007], and gas bubbles are released upon slight sediment disturbance [*MacDonald et al.*, 2003]. Sassen et al. [2001] recovered thermogenic gas hydrates from the mound with an average gas composition of 75.2% methane, 7.5% ethane, 11.2% propane, 5.5% isobutane, and 0.5% n-butane. MacDonald et al. [2003] observed carbonate chimneys, active oil seepage, and a chemosynthetic community that clusters away from the center of the mound with the submarine *Alvin*. Synethic-aperture-radar (SAR) images document persistent oil seepage on the ocean surface above the vent [*Garcia-Pineda et al.*, 2012].

I characterize the vent using three-dimensional seismic data, temperature-gradient measurements from Ruppel et al. [2005], and subsurface pore-water salinity measurements from Ruppel et al. [2005] and Paull et al. [2005]. These data show that, beneath the vent, there is an incredible shoaling of the BSR and that salinity and temperature gradients are significantly higher than background levels. I model the coexistence of an uplifted BSR, high salinities, and elevated temperature gradients with two approaches in two separate chapters.

In Chapter 2, I assume that high salinity fluids are generated by the dissolution of salt bodies at depth and that hot, saline fluids are expelled vertically. I show that this model can explain the observed salinity, temperature, and BSR if the flux of gas is 30x larger than the flux of water by volume. The key findings of this chapter are that: 1) I present a model that reconciles both salinity and temperature anomalies at a deepwater vent for the first time, and 2) I present a model that can be used to calculate water and hydrocarbon flux from deepwater vents around the world where geochemical and temperature-gradient data are available.

Chapter 3 is a continuation of Chapter 2. In Chapter 2, I show that the salinity and temperature signature at vents can be explained by the upward flow of gas and water from depth. My model predicts a volumetric gas flux that is 30x greater than the volumetric water flux and estimates the base of the hydrate stability zone (i.e. BSR depth) to be 25 meters below seafloor (mbsf). The paradox of this conclusion is that if gas and water are flowing vertically together and the base of the hydrate stability zone is beneath the seafloor, then hydrate solidification will occur, generating heat and salt. This insight, inferred from numerical modeling, is corroborated by field studies which have collected

hydrates on the vent [*Ruppel et al.*, 2005; *Sassen et al.*, 2001; *Winters et al.*, 2007] and recorded slight salinity increases with decreasing depth beneath the vent [*Paull et al.*, 2005; *Ruppel et al.*, 2005], consistent with salt exclusion during hydrate formation [*Liu and Flemings*, 2006]. Thus, in Chapter 3, I address the likelihood of heat and salt generation via hydrate formation.

I use the model developed by Liu and Flemings [2007] to simulate hydrate solidification during the upward flow of gas. In this model, free gas combines with water to form hydrate: salt is excluded and latent heat is released, resulting in the generation of a warm, saline brine near the seafloor. Chapter 3 is significant because it presents the first venting model that simulates both the release of heat and the exclusion of salt during hydrate solidification.

The application of this work is far-reaching. It directly addresses the interrelation of high salinities, elevated temperature gradients, gas hydrates, and fluid expulsion observed at deepwater vents. A better understanding of vent processes and vent fluid fluxes is critical for researchers who study vent ecosystems [*Hornbach et al.*, 2007; *MacDonald et al.*, 2004; *Niemann et al.*, 2006; *Paull et al.*, 1984]. Furthermore, a better understanding of vent processes in the deepwater will have direct impact on our understanding of the evolving behavior of gas vents and hydrate systems in the Arctic [*Shakhova et al.*, 2010].

The hydrocarbon flux estimates presented in Chapter 2 revitalize the hypothesis that hydrocarbon flux from deepwater vents has been significantly underestimated [*Milkov et al.*, 2003] and that it may influence oceanic and atmospheric carbon budgets

[*Judd et al.*, 2002; *Milkov et al.*, 2003]. The linkage between natural hydrocarbon seepage, the Gulf's rapid biodegradation of hydrocarbons [*Hazen et al.*, 2010; *Kessler et al.*, 2011b], and deepwater oxygen anomalies [*Joye et al.*, 2011; *Kessler et al.*, 2011a; *Kessler et al.*, 2011b] observed after the *Deepwater Horizon* oil spill remains poorly understood. Natural vents have been acknowledged as a potential explanation for the rapid biodegradation of hydrocarbons [*Hazen et al.*, 2010] and deepwater oxygen anomalies [*Joye et al.*, 2011] observed after the oil spill. My extraordinarily large hydrocarbon flux estimates imply that natural seepage may explain some of these observations

Future studies should develop two-dimensional and three-dimensional numerical models to describe the venting process. Field studies should document the geochemical and thermal signature at vents in high latitudes, so that the approach presented here can be applied to the Arctic, a region undergoing rapid environmental change [e.g. *Shakhova et al.*, 2010]. Finally, future efforts should develop systematic relationships between fluid fluxes and the microbial communities observed at vents [e.g. *Niemann et al.*, 2006]. These relationships will reveal how methane biofilters may change for different fluid fluxes and at different latitudes, elucidating the role of microbial communities as a methane sink.

REFERENCES

Bangs, N. L. B., D. S. Sawyer, and X. Golovchenko (1993), Free gas at the base of the gas hydrate zone in the vicinity of the Chile triple junction, *Geology*, *21*(10), 905-908.

Bredehoeft, J. D., and I. S. Papaopulos (1965), Rates of vertical groundwater movement estimated from the Earth's thermal profile, *Water Resour. Res.*, *1*(2), 325-328.

Brooks, J. M., H. B. Cox, W. R. Bryant, M. C. Kennicutt Ii, R. G. Mann, and T. J. McDonald (1986), Association of gas hydrates and oil seepage in the Gulf of Mexico, *Organic Geochemistry*, *10*(1–3), 221-234.

Dickens, G. R. (2003), Rethinking the global carbon cycle with a large, dynamic and microbially mediated gas hydrate capacitor, *Earth and Planetary Science Letters*, *213*(3-4), 169-183.

Garcia-Pineda, O., I. R. Macdonald, and D. Villa (2012), Natural Hydrocarbon Seepage Studies in the Gulf of Mexico, edited.

Hanor, J. S., and J. A. Mercer (2010), Spatial variations in the salinity of pore waters in northern deep water Gulf of Mexico sediments: implications for pathways and mechanisms of solute transport, *Geofluids*, *10*(1-2), 83-93.

Hazen, T. C., et al. (2010), Deep-Sea Oil Plume Enriches Indigenous Oil-Degrading Bacteria, *Science*, *330*(6001), 204-208.

Hornafius, J. S., D. Quigley, and B. P. Luyendyk (1999), The world's most spectacular marine hydrocarbon seeps (Coal Oil Point, Santa Barbara Channel, California): Quantification of emissions, *Journal of Geophysical Research*, *104*, 703-711.

Hornbach, M. J., C. Ruppel, and C. L. Van Dover (2007), Three-dimensional structure of fluid conduits sustaining an active deep marine cold seep, *Geophys. Res. Lett.*, *34*(5), L05601.

Hornbach, M. J., C. Ruppel, D. M. Saffer, C. L. Van Dover, and W. S. Holbrook (2005), Coupled geophysical constraints on heat flow and fluid flux at a salt diapir, *Geophys. Res. Lett.*, *32*(24), L24617.

Joye, S. B., et al. (2011), Comment on "A Persistent Oxygen Anomaly Reveals the Fate of Spilled Methane in the Deep Gulf of Mexico", *Science*, *332*(6033), 1033.

Judd, A. G., M. Hovland, L. I. Dimitrov, S. García Gil, and V. Jukes (2002), The geological methane budget at Continental Margins and its influence on climate change, *Geofluids*, *2*(2), 109-126.

Kessler, J. D., D. L. Valentine, M. C. Redmond, and M. Du (2011a), Response to Comment on "A Persistent Oxygen Anomaly Reveals the Fate of Spilled Methane in the Deep Gulf of Mexico", *Science*, *332*(6033), 1033.

Kessler, J. D., et al. (2011b), A Persistent Oxygen Anomaly Reveals the Fate of Spilled Methane in the Deep Gulf of Mexico, *Science*, *331*(6015), 312-315.

Kopf, A. J. (2002), Significance of mud volcanism, *Rev. Geophys.*, *40*(2), 1005.

Leifer, I., and I. R. Macdonald (2003), Dynamics of the gas flux from shallow gas hydrate deposits: interaction between oily hydrate bubbles and the oceanic environment, *Earth and Planetary Science Letters*, *210*(3-4), 411-424.

Leifer, I., and J. Boles (2005), Turbine tent measurements of marine hydrocarbon seeps on subhourly timescales, *Journal of Geophysical Research*, *110*, 1-12.

Liu, X., and P. B. Flemings (2006), Passing gas through the hydrate stability zone at southern Hydrate Ridge, offshore Oregon, *Earth and Planetary Science Letters*, *241*(1-2), 211-226.

Liu, X., and P. B. Flemings (2007), Dynamic multiphase flow model of hydrate formation in marine sediments, *J. Geophys. Res.*, *112*(B3), B03101.

MacDonald, I. R., W. W. Sager, and M. B. Peccini (2003), Gas hydrate and chemosynthetic biota in mounded bathymetry at mid-slope hydrocarbon seeps: Northern Gulf of Mexico, *Marine Geology*, *198*(1-2), 133-158.

MacDonald, I. R., D. B. Buthman, W. W. Sager, M. B. Peccini, and N. L. Guinasso (2000), Pulsed oil discharge from a mud volcano, *Geology*, *28*(10), 907-910.

Macdonald, I. R., N. L. Guinasso, Jr., S. G. Ackleson, J. F. Amos, R. Duckworth, R. Sassen, and J. M. Brooks (1993), Natural Oil Slicks in the Gulf of Mexico Visible From Space, *J. Geophys. Res.*, *98*(C9), 16351-16364.

MacDonald, I. R., et al. (2004), Asphpalt volcanism and chemosynthetic life, Campeche Knolls, Gulf of Mexico, *Science*, *304*, 999-1002.

McManus, K. M., and J. S. Hanor (1993), Diagenetic evidence for massive evaporite dissolution, fluid flow, and mass transfer in the Louisiana Gulf Coast, *Geology*, *21*(8), 727-730.

Milkov, A. V., R. Sassen, T. V. Apanasovich, and F. G. Dadashev (2003), Global gas flux from mud volcanoes: A significant source of fossil methane in the atmosphere and the ocean, *Geophys. Res. Lett.*, *30*(2), 1037.

Niemann, H., et al. (2006), Novel microbial communities of the Haakon Mosby mud volcano and their role as a methane sink, *Nature*, *443*(7113), 854-858.

Paull, C., W. Ussler, T. Lorenson, W. Winters, and J. Dougherty (2005), Geochemical constraints on the distribution of gas hydrates in the Gulf of Mexico, *Geo-Marine Letters*, *25*(5), 273-280.

Paull, C., B. Hecker, R. Commeau, R. P. Freeman-Lynde, C. Neumann, W. P. Corso, S. Golubic, J. E. Hook, E. Sikes, and J. Curray (1984), Biological Communities at

the Florida Escarpment Resemble Hydrothermal Vent Taxa, *Science*, *226*(4677), 965-967.

Reitz, A., M. Haeckel, K. Wallmann, C. Hensen, and K. Heeschen (2007), Origin of salt-enriched pore fluids in the northern Gulf of Mexico, *Earth and Planetary Science Letters*, *259*(3-4), 266-282.

Ruppel, C., G. R. Dickens, D. G. Castellini, W. Gilhooly, and D. Lizarralde (2005), Heat and salt inhibition of gas hydrate formation in the northern Gulf of Mexico, *Geophys. Res. Lett.*, *32*(4), L04605.

Sassen, R., S. T. Sweet, A. V. Milkov, D. A. DeFreitas, and M. C. Kennicutt, II (2001), Thermogenic vent gas and gas hydrate in the Gulf of Mexico slope: Is gas hydrate decomposition significant?, *Geology*, *29*(2), 107-110.

Shakhova, N., I. Semiletov, A. Salyuk, V. Yusupov, D. Kosmach, and Ö. Gustafsson (2010), Extensive Methane Venting to the Atmosphere from Sediments of the East Siberian Arctic Shelf, *Science*, *327*(5970), 1246-1250.

Sloan, E. D. (1998), *Clathrate Hydrates of Natural Gases*, 2nd ed., 705 pp., Marcel Dekker, New York.

Solomon, E. A., M. Kastner, I. R. MacDonald, and I. Leifer (2009), Considerable methane fluxes to the atmosphere from hydrocarbon seeps in the Gulf of Mexico, *Nature Geosci*, *2*(8), 561-565.

Spieß, V., and N. Fekete (2011), Deep Sea Gas Flares and Associated Gas Hydrate Traps in the Shallow Subseafloor, in *7th International Conference on Gas Hydrates*, edited, Edinburgh, Scotland, UK.

Suess, E., et al. (1999), Gas hydrate destabilization: enhanced dewatering, benthic material turnover and large methane plumes at the Cascadia convergent margin, *Earth and Planetary Science Letters*, *170*(1-2), 1-15.

Valentine, D. L., D. C. Blanton, W. S. Reeburgh, and M. Kastner (2001), Water column methane oxidation adjacent to an area of active hydrate dissociation, Eel river Basin, *Geochimica et Cosmochimica Acta*, *65*(16), 2633-2640.

Wilson, A., and C. Ruppel (2007), Salt tectonics and shallow subseafloor fluid convection: models of coupled fluid-heat-salt transport, *Geofluids*, *7*(4), 377-386.

Winters, W. J., T. D. Lorenson, and C. K. Paull (2007), Initial Report of the IMAGES VIII/PAGE 127 Gas Hydrate and Paleoclimate Cruise on the RV Marion Dufresne in the Gulf of Mexico, 2-18 July 2002: U.S. Geological Survey Open-File Report 2004-1358, edited.

Wood, W. T., J. F. Gettrust, N. R. Chapman, G. D. Spence, and R. D. Hyndman (2002), Decreased stability of methane hydrates in marine sediments owing to phase-boundary roughness, *Nature*, *420*(6916), 656-660.

Xu, W., and C. Ruppel (1999), Predicting the occurrence, distribution, and evolution of methane gas hydrate in porous marine sediments, *J. Geophys. Res.*, *104*(B3), 5081-5095.

Chapter 2: HYDROCARBON FLUX FROM NATURAL DEEPWATER GULF OF MEXICO VENTS

ABSTRACT

Natural vents that expel water and hydrocarbons are present on continental margins around the world. The expelled fluids support biological communities, escape to the ocean and atmosphere, and may contribute significantly to oceanic and atmospheric carbon budgets. Studies of vents in the Gulf of Mexico have documented significant flow, high salinities, and elevated temperature gradients. Although several processes have been recognized that may contribute to increases in salinity and high temperature gradients at vents, a dominant process that explains both observations has not been described. Here I show that there is a unique water and hydrocarbon flux that simulates the observed salinity and temperature at deepwater vents. I estimate the hydrocarbon flux to be 6.0-9.9x10^4 t yr^{-1} from a single vent, and I extrapolate this to estimate the hydrocarbon flux from the entire Gulf of Mexico to be 3.4-5.5x10^7 t yr^{-1}. This flux is at least 100x greater than previous estimates and is 22-36% of the hydrocarbon flux from the Macondo oil spill. Large natural seepage may inoculate marine basins such as the Gulf of Mexico from oil spills like the 2010 *Deepwater Horizon* blowout by sustaining populations of hydrocarbon-degrading bacteria.

TEXT

I study the Ursa vent in ~1070 meters of water depth in the northern Gulf of Mexico (GoM) at lease blocks MC852/853 (Fig. 2.1). Synthetic-aperture-radar (SAR) images detect persistent residual oil seepage on the sea surface above the vent (Fig. 2.1) [*Garcia-Pineda et al.*, 2012]. Three-dimensional seismic data reveal that the vent is

Table 2.1: Nomenclature.

Symbol	*Name*	*Dimension**
C	Chloride concentration	$M\ L^{-3}$
c_{pw}	Heat capacity (water)	$L^2\ t^{-2}\ T^{-1}$
c_{pg}	Heat capacity (gas)	$L^2\ t^{-2}\ T^{-1}$
D	Diffusion coefficient	$L^2\ t^{-1}$
g	Acceleration due to gravity	$L\ t^{-2}$
k	Permeability	L^2
k_{rg}	Relative permeability of gas	Dimensionless
k_{rw}	Relative permeability of water	Dimensionless
L	Flow-path length	L
P	Pressure	$M\ t^{-2}\ L^{-1}$
P_w	Water-phase pressure	$M\ L^{-1}\ t^{-2}$
P^*_w	Overpressure	$M\ L^{-1}\ t^{-2}$
q_g	Gas flux	$L^3\ L^{-2}\ t^{-1}$
q_w	Water flux	$L^3\ L^{-2}\ t^{-1}$
S_{rg}	Irreducible gas saturation	Dimensionless
S_{rw}	Irreducible water saturation	Dimensionless
S_w	Water saturation	Dimensionless
T	Temperature	T
T_L	Temperature at source depth	T
T_U	Temperature at seafloor	T
z	Depth	L
λ	Bulk thermal conductivity	$M\ L\ t^{-3}\ T^{-1}$
μ_g	Gas viscosity	$M\ L^{-1}\ t^{-1}$
μ_w	Water viscosity	$M\ L^{-1}\ t^{-1}$
ρ_g	Gas density	$M\ L^{-3}$
ρ_w	Water density	$M\ L^{-3}$

*T=temperature; M=mass; t=time; L=length

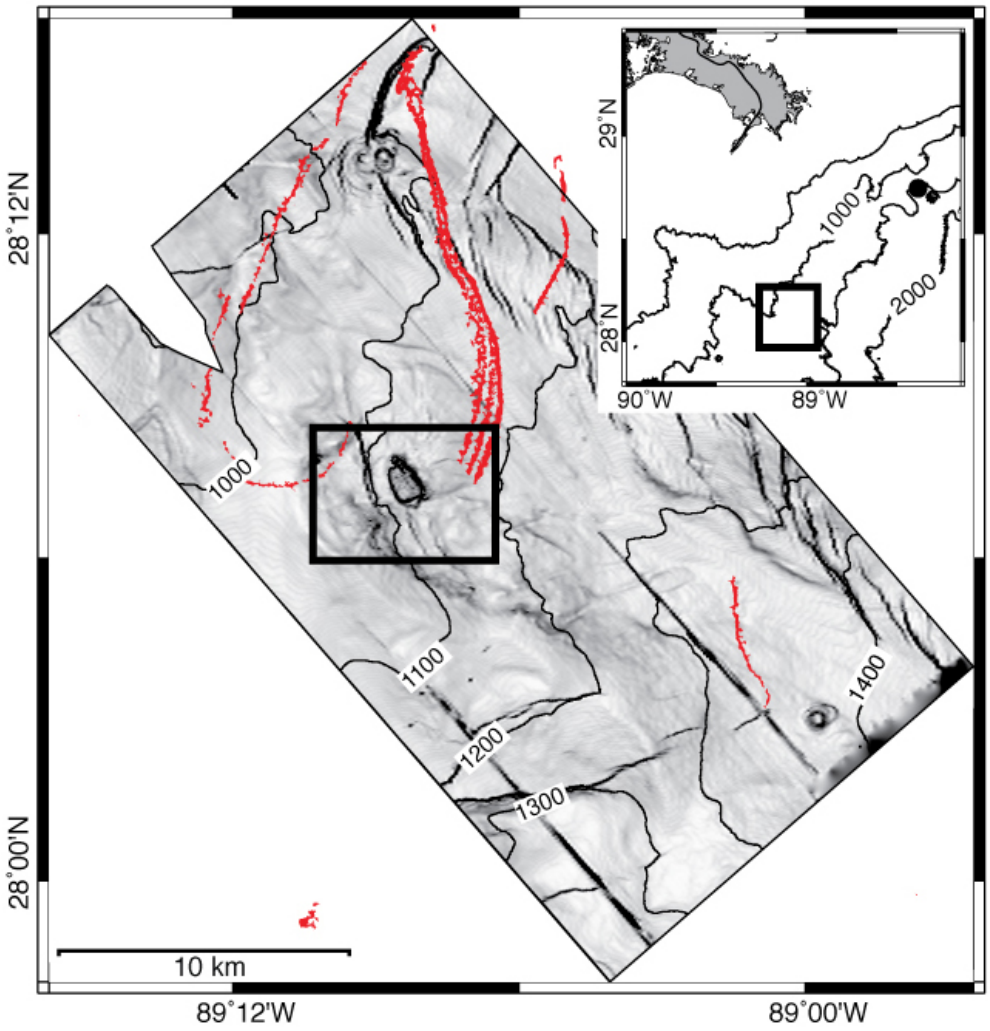

Figure 2.1. Seismic dip map of the Ursa Basin in the Gulf of Mexico.

Dip maps emphasize steeper gradients with darker colors. Contours are in meters below sea level (converted from time to depth assuming a 1.5 km s^{-1} acoustic velocity). Map is overlain with backscatter anomalies (red) detected from a SAR image taken May 24, 2006. Backscatter anomalies are interpreted as oil slicks on the ocean surface. The gas vent (black box, Fig. 2.2a) is ~220 km SSE of New Orleans and ~100 km from the Deepwater Horizon oil spill (black dot).

elevated ~75 meters above the seafloor and is roughly circular with a ~1.2 km diameter (Fig. 2.2a,b). A transparent zone centered underneath the vent extends to 1500 meters below seafloor (mbsf) (Fig. 2.2b); this zone is commonly interpreted to record the presence of gas [*Yin et al.*, 2003]. There is a strong, negative-polarity seismic reflection that rises rapidly at the vent's boundaries and is horizontal within a few meters of the seafloor beneath the vent edifice (Fig. 2.2b). I interpret that this reflection records a negative impedance contrast, marking the boundary between hydrate and water above and free gas and water below: it is the bottom-simulating reflector (BSR) [*Bangs et al.*, 1993]. Carbonate chimneys, active oil seepage, and a chemosynthetic community that clusters away from the center of the mound have been observed with submarine *Alvin* [*MacDonald et al.*, 2003]. Vent sediments are highly gas-charged [*MacDonald et al.*, 2003; *Winters et al.*, 2007], and gas bubbles are released upon slight disturbance of the mound [*MacDonald et al.*, 2003].

Chloride concentrations beneath the vent increase from seawater concentration (550 mM) to >4x seawater concentrations 1 mbsf (Fig. 2.2c) [*Paull et al.*, 2005; *C. Ruppel et al.*, 2005]. Temperature gradients measured in the first 3 mbsf within the vent (TM 5-9, TM 5-8) are ~15x the background geothermal gradient of 25 mK m^{-1} (Fig. 2.2d) [*C. Ruppel et al.*, 2005].

The vent is imaged as a transparent zone extending to a prominent salt diapir approximately 1500 mbsf (Fig. 2.2b). I envision that constant-temperature fluids are sourced at constant pressure from thick aquifer sands that onlap the salt diapir (Fig. 2.3). Pore pressures are held constant at the pressure necessary to hydraulically fracture the

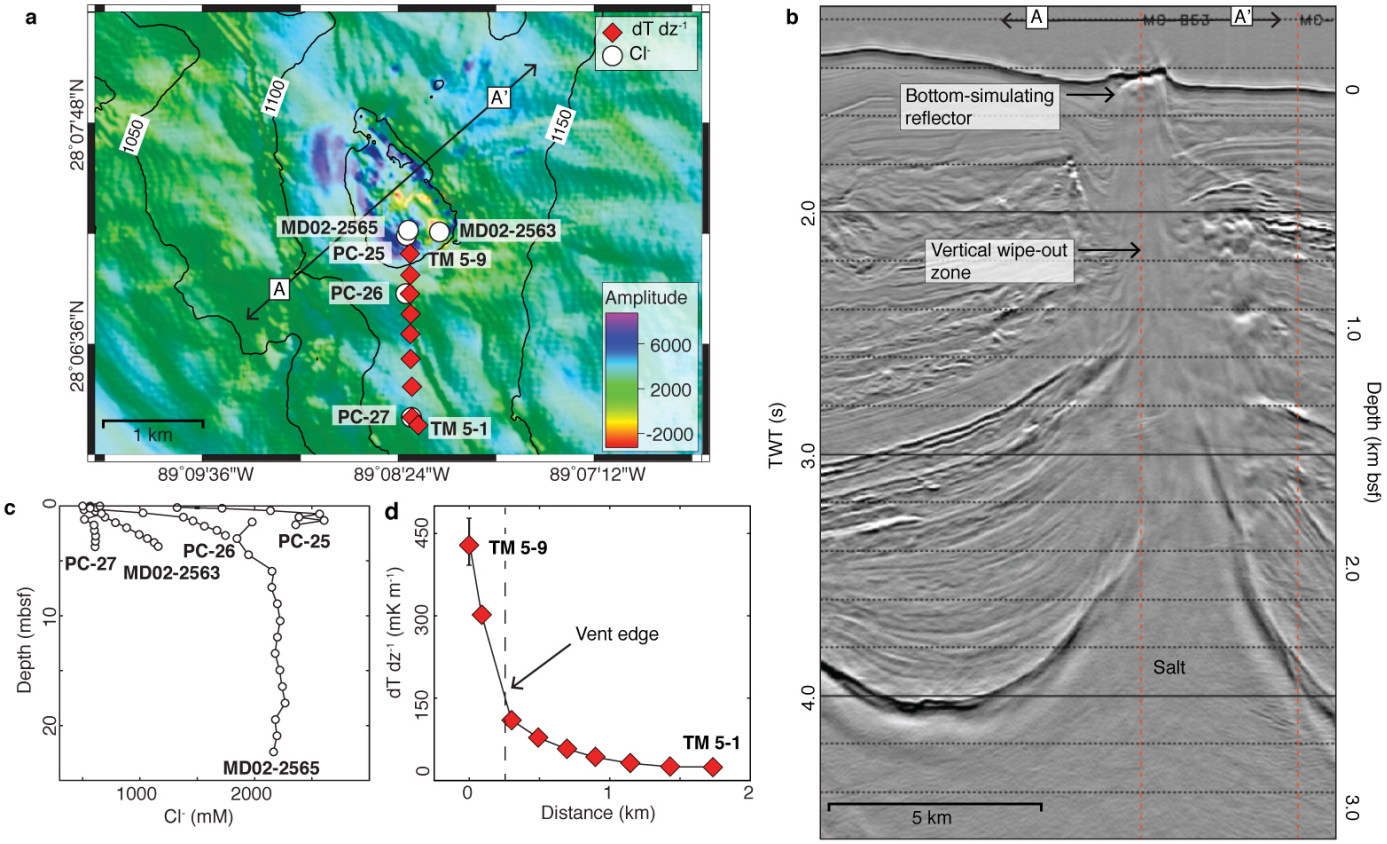

Figure 2.2. Subsurface plumbing, chloride measurements, and temperature gradients at MC852/853.

a, *Seafloor amplitudes showing locations of chloride and thermal-gradient measurements. Larger amplitudes (blue) likely record the presence of authigenic carbonates or hydrates. Negative amplitudes (yellow-red) record where the BSR intersects the seafloor. I interpret these areas to be where there is active gas venting.* ***b,*** *Seismic reflection profile through the gas vent with two-way travel time (TWT) and depth on vertical axes. TWT is converted to depth assuming an acoustic velocity of 2 km* s^{-1}. ***c,*** *Chloride gradients measured by piston and box core.* ***d,*** *Temperature gradients measured in upper 3 meters of the sediment column. Error bars are smaller than symbol size except at TM 5-9.*

cap rock at the crest of these aquifer sands [*Cathles and Smith*, 1983; *Hubbert and Willis*, 1972].

I model the coexistence of high salinities, elevated temperature gradients, and an uplifted BSR by assuming that high-salinity fluids are generated by dissolution of salt bodies at depth and that these warm, saline fluids are expelled vertically (Fig. 2.3). I assume one-dimensional and steady-state heat and salt transport. Material parameters of water and methane are assumed invariant. Chloride is transported by chemical diffusion and upward flow of water, and heat is transported by conduction and upward flow of water and free methane gas. I assume that water of constant salinity (~4.5x seawater) and gas are supplied at a constant rate from a depth of 1500 mbsf and that temperature at 1500 mbsf is 42.5 ^{o}C. At the seafloor, I assume seawater salinity and a temperature of 5 ^{o}C.

Chloride is transported solely by water, so I initially solve for the water flux (q_w) necessary to simulate the highest observed chloride gradient (PC-25). The chloride concentration with depth ($C(z)$) is described by (see Appendix A2):

$$C(z) = C_U + \left(C_L - C_U\right)\left(\frac{e^{\frac{q_w z}{D}} - 1}{e^{\frac{q_w L}{D}} - 1}\right) \tag{3.1}$$

where z is depth, L is flow-path length (1500 m), D is the diffusion coefficient scaled for diffusion in a porous media [*Domenico and Schwartz*, 1990; *Li and Gregory*, 1974], and C_U and C_L are Cl^- boundary conditions defined by the Cl^- concentration in seawater (550 mM) at the seafloor and the maximum observed Cl^- concentration (2600 mM) at the

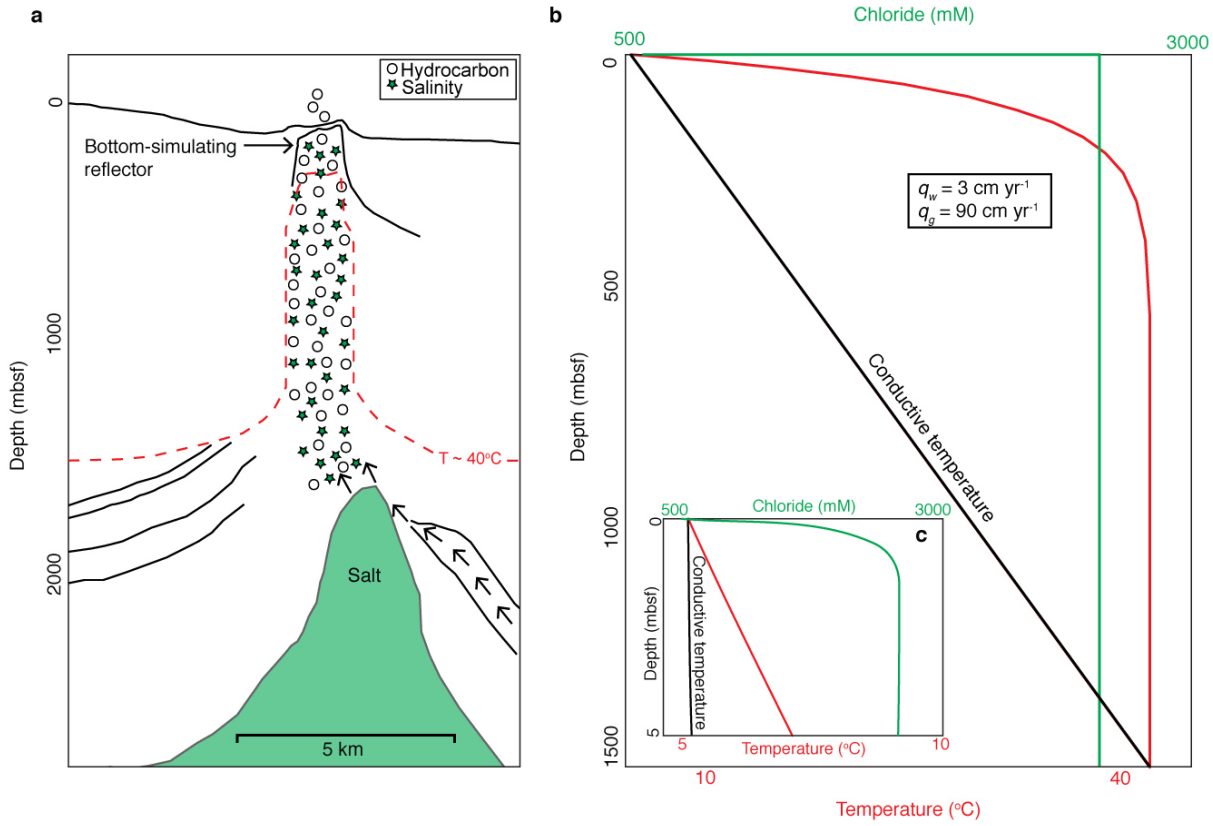

Figure 2.3. My view—a conceptual model.

a, *In the vent, high salinities and high temperatures record the upward flow of water and hydrocarbons from depth. We model the coexistence of high salinities, elevated temperature gradients, and an uplifted BSR by assuming that water and hydrocarbon are flowing vertically together. Water supplied from depth transports heat and salt (green stars), and hydrocarbon (white circles) transports heat.* ***b,*** *Simulated temperature-versus-depth and chloride-versus-depth profiles for an upward 3 cm yr^{-1} water flux (q_w) and 90 cm yr^{-1} gas flux (q_g) (equations 2.1 and 2.2). The isothermal and isohaline vent is advecting fluids at a rapid rate, making advection the dominant heat- and salt-transport process over conduction and diffusion.* ***c,*** *Same simulations as in part b plotted over a depth of 5 meters.*

source depth (see Table A2). To match the observed Cl^- gradient, a 3 cm yr^{-1} water flux is required (Fig. 2.4a).

Temperature as a function of depth (*T(z)*) is controlled by both water flux (q_w) and gas flux (q_g) (see Appendix A3):

$$T(z) = T_U + (T_L - T_U)\left(\frac{e^{\frac{q_w\rho_w c_{pw} z + q_g\rho_g c_{pg} z}{\lambda}} - 1}{e^{\frac{q_w\rho_w c_{pw} L + q_g\rho_g c_{pg} L}{\lambda}} - 1}\right) \tag{3.2}$$

where $\rho_w c_{pw}$ and $\rho_g c_{pg}$ are volumetric heat capacities of water and methane and λ is bulk thermal conductivity (see Table A3). The temperature at the seafloor (T_U) is 5 ^oC [*C. Ruppel et al.*, 2005; *Winters et al.*, 2007], and the temperature (T_L) at the 1500-mbsf source depth is 42.5 ^oC based on a background geothermal gradient of 25 mK m^{-1}. To simulate the highest observed temperature gradient of 435 mK m^{-1} (TM 5-9) within the upper 3 mbsf, a gas flux of 90 cm yr^{-1} must accompany the established 3 cm yr^{-1} water flux (Fig. 2.4b). This venting fluid results in a seafloor heat flux of 465 mW m^{-2}, which is ~19x greater than the background heat flux of ~25 mW m^{-2}.

I describe the upward flow of water and gas with a multiphase adaptation of Darcy's law (see Appendix A4):

$$q_w = \frac{k\left(\frac{S_w - S_{rw}}{1 - S_{rw} - S_{rg}}\right)^4}{\mu_w}\left(\frac{dP_w^*}{dz}\right), \tag{2.3}$$

$$q_g = \frac{k\left(1-\frac{S_w - S_{rw}}{1-S_{rw}-S_{rg}}\right)^2\left(1-\left(\frac{S_w - S_{rw}}{1-S_{rw}-S_{rg}}\right)^2\right)}{\mu_g}\left(\frac{dP_w^*}{dz} - g\left(\rho_w - \rho_g\right)\right). \quad (2.4)$$

$dP^*_w\, dz^{-1}$ is the water-phase overpressure gradient, ρ_w and ρ_g are water and gas density, g is the acceleration due to gravity, k is permeability, μ_w and μ_g are water and gas viscosity, S_w is water saturation, and S_{rw} and S_{rg} are irreducible (i.e. minimal) water and gas saturations (see Table A4). I simulate the water saturation and pressure gradient that result at a range of permeabilities for the 3 cm yr^{-1} water flux and 90 cm yr^{-1} gas flux I infer to be present (Fig. 2.4c). I find that for a range of permeabilities, the water saturation lies between 0.67 and 0.96 even though the flux of gas is 30x that of water. This is because gas viscosity and density are significantly lower than those of water. If the overpressure gradient equals the overburden gradient (~10^4 Pa m^{-1}), as has been observed at other vents [*Reilly and Flemings*, 2010; *Tréhu et al.*, 2004], then the water saturation is 0.71 and the permeability is 4.4×10^{-16} m^2. This permeability is within the range observed near the seafloor [*Schneider*, 2011].

A 3 cm yr^{-1} water flux and 90 cm yr^{-1} gas flux equates to a volume flux of 2.4×10^4 m^3 yr^{-1} for water and 7.1×10^5 m^3 yr^{-1} for gas if fluxes are assumed constant over the area of the shoaled BSR (~0.79 km^2). For the assumed fluid densities (see Table A3), I find the mass flux of water and gas to be 2.4×10^4 t yr^{-1} and 6.0×10^4 t yr^{-1} for the MC852/853 vent. If instead of gas and water, oil and water are expelled at MC852/853; my model predicts an even greater hydrocarbon mass flux: 9.9×10^4 t yr^{-1}. It is most likely that water, oil, and gas flow together; therefore I adopt the 6.0×10^4 t yr^{-1} gas flux and 9.9×10^4 t yr^{-1} oil flux as two end members for hydrocarbon discharge.

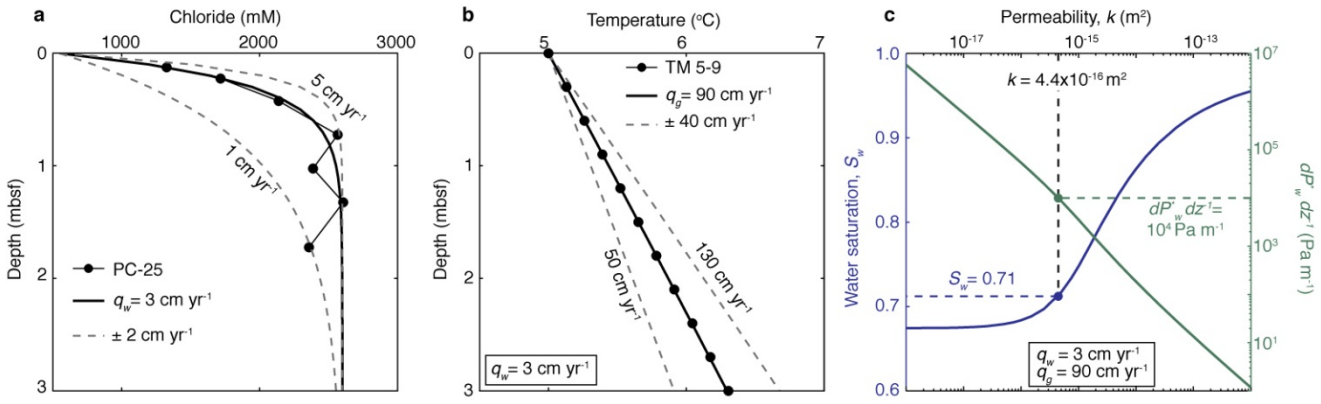

Figure 2.4. Implications of chloride and temperature observations.

a, *A 3 cm yr^{-1} water flux is the optimal flux to explain chloride anomalies.* ***b,*** *An additional gas flux of 90 cm yr^{-1} is needed to also simulate the 435 mK m^{-1} thermal gradient measured at TM 5-9.* ***c,*** *Plot shows the unique water saturation and overpressure gradient that will drive a 3 cm yr^{-1} water flux and 90 cm yr^{-1} gas flux for different permeabilities. An overpressure gradient of 10^{4} Pa m^{-1} implies a permeability of 4.4x10^{-16} m^{2}.*

For comparison, video-imaging techniques have been used to quantify hydrocarbon mass fluxes as high as $2.7x10^{1}$ t yr^{-1} from a single GoM vent [*Leifer and Macdonald*, 2003]; however, this technique does not measure flow over long timescales and only quantifies flux from a localized seep point, not an entire vent. Using a statistical approach, it was estimated that the average hydrocarbon flux from any given deepwater vent around the world is $5.4x10^{3}$ t yr^{-1} [*Milkov et al.*, 2003], which is 5-9% of my estimated flux.

In the GoM, there are 559 vents creating persistent slicks [*Garcia et al.*, 2009], and if each vent expels hydrocarbons at the rate of my prediction at MC852/853, then the GoM hydrocarbon seepage rate is $3.4\text{-}5.5x10^{7}$ t yr^{-1}. This value is at least 100x greater than previous studies that estimate GoM seepage ranging from $8\text{-}20x10^{4}$ t yr^{-1} using remote sensing [*NRC*, 2003].

My estimated hydrocarbon mass flux from MC852/853 is 0.04-0.06% of the average mass flux at the *Deepwater Horizon* oil spill ($1.54x10^{8}$ t yr^{-1}) [*McNutt et al.*, 2011], and my GoM seepage rate is 22-36% of this average discharge rate [*McNutt et al.*, 2011]. The implications of my flux estimates are twofold. First, natural hydrocarbon flux into the world's oceans may be far greater than previously thought, impacting our understanding of the carbon cycle and its implications for both climate and biological systems. Conversely, basins with a large natural hydrocarbon flux may fertilize an indigenous population of hydrocarbon-degrading bacteria [*Hazen et al.*, 2010]. In these environments, there is an extant population which can rapidly proliferate and consume hydrocarbons expelled during accidents such as the *Deepwater Horizon* event [*Hazen et al.*, 2010; *Kessler et al.*, 2011; *Valentine et al.*, 2012].

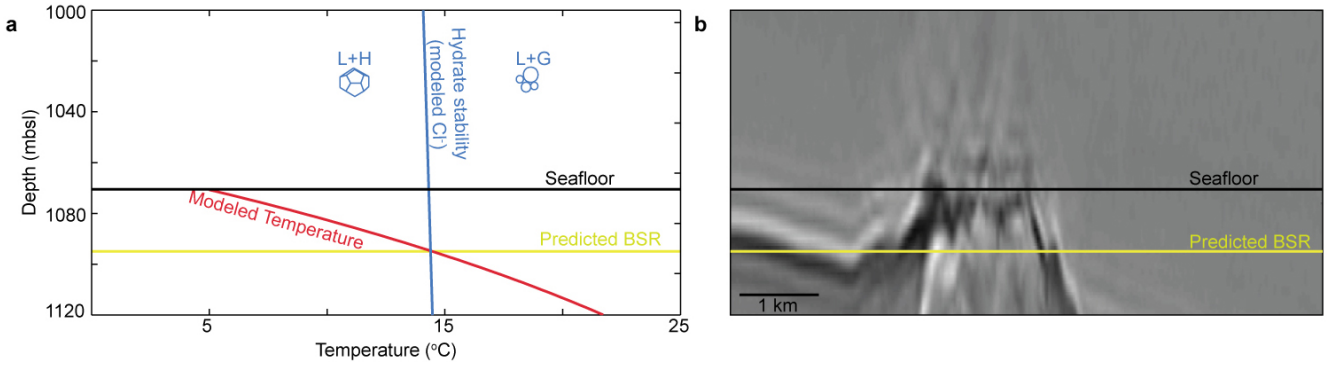

Figure 2.5. Agreement between model results and observed hydrate stability depth.

a, *Seafloor depth (black) indicates the depth at which measurement TM 5-9 was taken (1070 mbsl). The three-phase hydrate stability curve (blue) plots pressures and temperatures at which hydrate (H), liquid (L), and gas (G) coexist. I calculate the hydrate equilibrium curve with the CSMHyd hydrate model[Sloan, 1998], using average gas composition from hydrates collected on the vent [Sassen et al., 2001] and the modeled Cl^- concentrations converted to salinity (Fig. 2.4a). Pressures are converted to depth assuming hydrostatic pressure conditions through both the water and sediment column. The in-situ thermal gradient (red) is calculated using the modeled temperature profile (Fig. 2.4b). The intersection of the hydrate stability curve and the thermal gradient predicts the base of the hydrate stability zone to be ~25 mbsf (yellow).* ***b,*** *Seismic reflection profile through the vent. Two-way travel time is converted to depth assuming an acoustic velocity of 2 km s^{-1} below seafloor. The calculated base of the hydrate stability zone shows good agreement with the BSR depth observed in seismic data.*

My model is one-dimensional, yet heat and salt may also be transported laterally. However, because thermal diffusivity is several orders of magnitude larger than chemical diffusivity [*Liu and Flemings*, 2006], a two-dimensional model will require an even greater hydrocarbon flux to explain the high temperature gradient near the seafloor. I assume steady-state conditions even though vent flow can vary spatially and temporally [*Hu et al.*, 2012; *MacDonald et al.*, 2000]. However, based on the presence of mature biological vent communities [*MacDonald et al.*, 2003], persistent oil slicks on the sea surface above vents [*Garcia-Pineda et al.*, 2012], and consistently high temperature and salinity in multiple vents [*C. Ruppel et al.*, 2005], I infer constant discharge over long time scales. In addition, the depth of three-phase (liquid-gas-hydrate) hydrate stability predicted from my model is in good agreement with the observed base of the hydrate stability zone (Fig. 2.5), lending credence to the modeling approach. Finally, I recognize that significant hydrate solidification in gas systems will produce higher salinities and elevated temperatures [*Liu and Flemings*, 2006]. I assume, however, that these effects are secondary and beyond the scope of the study.

I present an approach for estimating the mass flux of hydrocarbons from the seafloor. The predicted mass fluxes are more than 100x greater than previously estimated in the GoM [*NRC*, 2003] and perhaps other oceans. In certain marine basins, a deep-sea microbial community may adapt to large, steady natural hydrocarbon seepage over time [*Hazen et al.*, 2010]. These microbial communities may account for the rapid hydrocarbon biodegradation rates observed after the *Deepwater Horizon* spill [*Hazen et al.*, 2010; *Kessler et al.*, 2011; *Valentine et al.*, 2012].

REFERENCES

Bangs, N. L. B., D. S. Sawyer, and X. Golovchenko (1993), Free gas at the base of the gas hydrate zone in the vicinity of the Chile triple junction, Geology, 21(10), 905-908.

Cathles, L. M., and A. T. Smith (1983), Thermal constraints on the formation of mississippi valley-type lead-zinc deposits and their implications for episodic basin dewatering and deposit genesis, Economic Geology, 78(5), 983-1002.

Domenico, P. A., and F. W. Schwartz (1990), Physical and chemical hydrogeology, 824 pp., John Wiley & Sons, New York.

Garcia-Pineda, O., I. R. Macdonald, and D. Villa (2012), Natural Hydrocarbon Seepage Studies in the Gulf of Mexico, edited.

Garcia, O., I. R. MacDonald, B. Zimmer, W. Shedd, and M. Frye (2009), Satellite SAR inventory of Gulf of Mexico oil seeps and shallow gas hydrates, paper presented at EGU General Assembly, Vienna, Austria.

Hazen, T. C., et al. (2010), Deep-Sea Oil Plume Enriches Indigenous Oil-Degrading Bacteria, Science, 330(6001), 204-208.

Hu, L., S. A. Yvon-Lewis, J. D. Kessler, and I. R. MacDonald (2012), Methane fluxes to the atmosphere from deepwater hydrocarbon seeps in the northern Gulf of Mexico, J. Geophys. Res., 117(C1), C01009.

Hubbert, M. K., and D. G. Willis (1972), Mechanics of hydraulic fracturing, Mem. - Am. Assoc. Pet. Geol., 18, 239-257.

Kessler, J. D., et al. (2011), A Persistent Oxygen Anomaly Reveals the Fate of Spilled Methane in the Deep Gulf of Mexico, Science, 331(6015), 312-315.

Leifer, I., and I. R. Macdonald (2003), Dynamics of the gas flux from shallow gas hydrate deposits: interaction between oily hydrate bubbles and the oceanic environment, Earth and Planetary Science Letters, 210(3-4), 411-424.

Li, Y.-H., and S. Gregory (1974), Diffusion of ions in sea water and in deep-sea sediments, Geochimica et Cosmochimica Acta, 38(5), 703-714.

Liu, X., and P. B. Flemings (2006), Passing gas through the hydrate stability zone at southern Hydrate Ridge, offshore Oregon, Earth and Planetary Science Letters, 241(1-2), 211-226.

MacDonald, I. R., W. W. Sager, and M. B. Peccini (2003), Gas hydrate and chemosynthetic biota in mounded bathymetry at mid-slope hydrocarbon seeps: Northern Gulf of Mexico, Marine Geology, 198(1-2), 133-158.

MacDonald, I. R., D. B. Buthman, W. W. Sager, M. B. Peccini, and N. L. Guinasso (2000), Pulsed oil discharge from a mud volcano, Geology, 28(10), 907-910.

McNutt, M., R. Camilli, G. Guthrie, P. Hsieh, V. Labson, B. Lehr, D. Maclay, A. Ratzel, and M. Sogge (2011), Assessment of Flow Rate Estimates for the Deepwater Horizon / Macondo Well Oil SpillRep., National Incident Command, Interagency Solutions Group.

Milkov, A. V., R. Sassen, T. V. Apanasovich, and F. G. Dadashev (2003), Global gas flux from mud volcanoes: A significant source of fossil methane in the atmosphere and the ocean, Geophys. Res. Lett., 30(2), 1037.

NRC (2003), Oil in the sea III : inputs, fates, and effects National Academies Press, Washington D.C.

Paull, C., W. Ussler, T. Lorenson, W. Winters, and J. Dougherty (2005), Geochemical constraints on the distribution of gas hydrates in the Gulf of Mexico, Geo-Marine Letters, 25(5), 273-280.

Reilly, M. J., and P. B. Flemings (2010), Deep pore pressures and seafloor venting in the Auger Basin, Gulf of Mexico, Basin Res. Basin Research, 22(4), 380-397.

Ruppel, C., D. Lizarralde, G. Dickens, and K. Brown (2005), Northern Gulf of Mexico Gas Hydrates (IODP #554): LDEO Site Survey Data Bank Submission Based on NSF-ODP Funded Cruise, edited.

Ruppel, C., G. R. Dickens, D. G. Castellini, W. Gilhooly, and D. Lizarralde (2005), Heat and salt inhibition of gas hydrate formation in the northern Gulf of Mexico, Geophys. Res. Lett., 32(4), L04605.

Sassen, R., S. T. Sweet, A. V. Milkov, D. A. DeFreitas, and M. C. Kennicutt, II (2001), Thermogenic vent gas and gas hydrate in the Gulf of Mexico slope: Is gas hydrate decomposition significant?, Geology, 29(2), 107-110.

Schneider, J. (2011), Compression and permeability behavior of natural mudstones, 302 pp, University of Texas at Austin, Austin.

Sloan, E. D. (1998), Clathrate Hydrates of Natural Gases, 2nd ed., 705 pp., Marcel Dekker, New York.

Tréhu, A. M., P. B. Flemings, N. L. Bangs, J. Chevallier, E. Gràcia, J. E. Johnson, C. S. Liu, X. Liu, M. Riedel, and M. E. Torres (2004), Feeding methane vents and gas hydrate deposits at south Hydrate Ridge, Geophys. Res. Lett., 31(23), L23310.

Valentine, D. L., I. Mezić, S. Maćešić, N. Črnjarić-Žic, S. Ivić, P. J. Hogan, V. A. Fonoberov, and S. Loire (2012), Dynamic autoinoculation and the microbial ecology of a deep water hydrocarbon irruption, Proceedings of the National Academy of Sciences.

Winters, W. J., T. D. Lorenson, and C. K. Paull (2007), Initial Report of the IMAGES VIII/PAGE 127 Gas Hydrate and Paleoclimate Cruise on the RV Marion Dufresne in the Gulf of Mexico, 2-18 July 2002: U.S. Geological Survey Open-File Report 2004-1358, edited.

Yin, P., S. Berné, P. Vagner, B. Loubrieu, and Z. Liu (2003), Mud volcanoes at the shelf margin of the East China Sea, Marine Geology, 194(3-4), 135-149.

Chapter 3: HEAT AND SALT GENERATION BY HYDRATE SOLIDIFATION AT DEEPWATER GULF OF MEXICO VENTS

ABSTRACT

I present two models of gas venting through the hydrate stability zone at the Ursa vent in 1070 meters water depth in the northern Gulf of Mexico. First, I present an equilibrium model in which free gas supplied from depth forms hydrate, excludes salt, and releases heat until pore water is too warm and saline for further hydrate formation. The model self-generates three-phase equilibrium from the base of the hydrate stability zone to the seafloor. The model is a simple approximation technique to simulate hydrate formation given no volume expansion, no chemical diffusion, and no transport of the liquid phase. I then extend this basic equilibrium model with a one-dimensional, multicomponent, multiphase, fluid- and heat-flow model developed by Liu and Flemings [2007] to describe hydrate formation at the Ursa vent. In this model, free gas supplied from depth combines with water to form hydrate: salt is excluded and heat is released, resulting in the generation of a warm, saline brine near the seafloor. The model predicts a salinity profile that is distinct from that which is simulated by deep advection. Simulated temperature gradients, however, are similar to those predicted by the deep-advection model. A better understanding of the hydrogeological processes at deepwater vents is important for estimating their global input of heat, mass, and carbon.

1. INTRODUCTION

Gas hydrate is an ice-like, crystalline compound that contains methane and other light gases in a lattice of water molecules [*Sloan*, 1998]. It is naturally found along continental margins in water depths > ~400 m, where there are high pressures, low temperatures, and ample supplies of gas and water [*Kvenvolden*, 1993]. Gas hydrates may

host economic quantities of natural gas [*Milkov and Sassen*, 2002]. Their dissociation may have contributed to past environmental change [*Dickens*, 2003] and may be causing ongoing methane release to the atmosphere in the Arctic [*Kort et al.*, 2012; *Shakhova et al.*, 2010]. Hydrate decomposition in marine sediments may rapidly elevate pore pressure, prompting slope failure along continental margins [*Kayen and Lee*, 1991].

High concentrations of hydrate exist in near-seafloor sediments at gas venting locations around the world [*Brooks et al.*, 1986; *Judd*, 2003]. These vents are at water depths within the regional hydrate stability zone (RHSZ), and yet gas bubbles emanate from the seeps [*Greinert et al.*, 2006; *Haeckel et al.*, 2004; *Judd*, 2003; *MacDonald et al.*, 2003; *C K Paull et al.*, 1995; *Tréhu et al.*, 2004]. In seismic data, the bottom-simulating reflector (BSR), which marks the boundary between hydrate and water above and gas and water below [*Bangs et al.*, 1993], rises toward the seafloor at the center of vents [*Bünz and Mienert*, 2004; *Hornbach et al.*, 2005; *Spieß and Fekete*, 2011; *Tréhu et al.*, 2004; *Wood et al.*, 2002]. These uplifted BSRs are commonly interpreted to record the presence of free gas within the RHSZ [*Liu and Flemings*, 2006; *Tréhu et al.*, 2004; *Yin et al.*, 2003]. Numerous mechanisms of free-gas transport through the RHSZ have been proposed such as: hydrofracturing and critical gas pressures below the RHSZ [*Flemings et al.*, 2003; *Torres et al.*, 2011], the formation of an oily or hydrate layer around bubbles that isolates gas from the surrounding water [*MacDonald et al.*, 2003], the inhibition of hydrate formation by localized elevations in salinity and/or temperature [*Liu and Flemings*, 2006; *Milkov et al.*, 2004], local dehydration of sediments [*Tréhu et al.*, 2004], and the inhibition of hydrate formation by capillary forces [*Clennell et al.*, 1999].

Several studies have documented elevated salinities and high temperatures near the seafloor of hydrate-bearing vents with direct subsurface measurements [e.g. *Ruppel et al.*, 2005] and electromagnetic surveying [e.g. *Ellis et al.*, 2008]. Piston cores collected on vent edifices exhibit concave-downward salinity curves [*C Paull et al.*, 2005; *Reitz et al.*, 2007; *Ruppel et al.*, 2005], whereas subsurface measurements made on vent flanks record concave-upward salinity and temperature profiles [*Ruppel et al.*, 2005]. Other studies have documented elevated in-situ salinities that lie on the three-phase hydrate stability boundary at the Cascadia accretionary margin [*Liu and Flemings*, 2006] and at the Mallick hydrate reservoir [*Wright et al.*, 2005].

Although the coexistence of gas hydrates, free-gas expulsion, an uplifted BSR, and high salinities and temperatures has been well documented at vents, conclusive evidence of the origin of these phenomena has remained elusive. A number of studies have assumed that high salinities, elevated temperatures, and an uplifted BSR record the upward flow of warm, salty fluids from depth [*Hornbach et al.*, 2005; *Ruppel et al.*, 2005; *Wood et al.*, 2002]. This approach is corroborated by concave-down geochemical profiles [*C Paull et al.*, 2005; *Reitz et al.*, 2007; *Ruppel et al.*, 2005], which provide evidence for advective flow. Additionally, the widespread occurrence of salt domes and deep-seated faults in marine basins such as the Gulf of Mexico (GoM) suggests that high salinities at vents are produced by dissolution and transport of salt from underlying salt bodies. This model, however, cannot explicitly explain observations of high-saturation hydrate deposits at vents [*Haeckel et al.*, 2004; *Torres et al.*, 2004] or increases in salinity with decreasing depth [*Liu and Flemings*, 2006; *Ruppel et al.*, 2005; *Winters et al.*, 2007]. Furthermore, simple numerical models have shown that there is a fundamental mismatch in the upward fluid-flow rates necessary to explain observed temperature and

geochemical gradients at vents *[Hornbach et al., 2005; Smith et al., 2011]*. Finally, the deep-advection model cannot explain how free gas passes through the RHSZ to the seafloor since it commonly predicts the depth of hydrate stability to be below the seafloor [*Hornbach et al.*, 2005; *Ruppel et al.*, 2005; *Smith et al.*, 2011].

An alternative mechanism for heat and salt generation at vents is hydrate solidification. In this model, salt is elevated via the exclusion of salt during hydrate formation [*Tréhu et al.*, 2004], and latent heat is released [*Cathles and Chen*, 2004]. The majority of numerical models describing this process assume that methane is only transported in the dissolved phase [*Buffett and Zatsepina*, 2000; *Davie and Buffett*, 2001; *Hyndman and Davis*, 1992; *Xu and Ruppel*, 1999]. In these models, hydrate-formation rates are very slow, and thus, hydrate formation will not significantly perturb pressure, temperature, and salinity conditions within the system [*Liu and Flemings*, 2007; *Xu and Ruppel*, 1999]. These models are appropriate for settings in which the gas flux is low compared to the water flux and in which there is no free gas in the RHSZ.

These models, however, are not applicable to settings such as: GoM vents [*Cathles and Chen*, 2004; *MacDonald et al.*, 2003], Hydrate Ridge [*Tréhu et al.*, 2004], Blake Ridge [*C K Paull et al.*, 1995], or the Black Sea [*Kessler et al.*, 2006], where free gas actively vents through the hydrate stability zone. To model these sites of high free-gas flux, Liu and Flemings [2006; 2007] present a model in which free gas combines with water to form hydrate. In this model, hydrate-formation rates are sufficiently high to generate hyper-saline pore water that shifts the three-phase hydrate stability boundary to the seafloor, permitting free-gas expulsion [*Liu and Flemings*, 2006; 2007]. Daigle and Dugan [2010] extend this model to account for the fracture generation that is common for

multiphase flow [*Jain and Juanes*, 2009]. These models offer a comprehensive explanation for the enigmatic coexistence of elevated salinities, high hydrate saturations, free-gas expulsion at the seafloor, and chimney-like features within the RHSZ; however, they do not account for the heat added by hydrate formation, which is a significant fraction of background heat flow [*Cathles and Chen*, 2004; *Liu and Flemings*, 2006].

Here I explore the hypothesis that hydrate formation generates warm, saline pore water that shifts the three-phase stability boundary to the seafloor. I first present an equilibrium model to describe how high salinities and temperatures can extend the three-phase zone from the base of the RHSZ to the seafloor. I then use the same dynamic multiphase-flow model of hydrate formation developed by Liu and Flemings [2007], except that I consider heat released during hydrate solidification. I simulate temperature, salinity, gas-saturation, and hydrate-saturation profiles during the upward migration of gas. The model predicts salinity profiles that are different from those simulated by deep advection. The temperature gradients produced by the model are similar to those predicted by deep advection.

Table 3.1: Nomenclature.

Symbol	*Name*	*Dimension**
C	Salinity	dimensionless
$c_{b,h,s,w}$	Heat capacity (bulk, hydrate, sediment, water)	$L^2\ t^{-2}\ T^{-1}$
C_{eq}	Equilibrium salinity at depth z	dimensionless
C_i	Initial salinity	dimensionless
D_s	Diffusion coefficient of salt	dimensionless
L	Latent heat	$L^2\ t^{-2}$
P	Pressure	$M\ t^{-2}\ L^{-1}$
q_e	Heat flux	$M\ L^2\ t^{-3}$
S_g	Gas saturation	dimensionless
S_h	Hydrate saturation	dimensionless
T	Temperature	T
t	Time	T
z	Depth	L
$\rho_{b,h,s,w}$	Density (bulk, hydrate, sediment, water)	$M\ L^{-3}$
ϕ	Porosity	dimensionless

*T=temperature; M=mass; t=time; L=length

2. EQUILIBRIUM MODELS

I model pressure and temperature conditions similar to those at the Ursa vent at lease blocks MC852/853 in the northern Gulf of Mexico. The vent is 1070 meters below sea level (mbsl). Seafloor temperature is ~5 ^{o}C, and the background geothermal gradient is 25 ^{o}C km^{-1} [*Ruppel et al.*, 2005]. I assume that the sediment column is hydrostatically pressured, that methane is the only natural gas present, and that pore water initially has seawater salinity (3.5%). Under these conditions, the base of the RHSZ is ~ 440 meters below seafloor (mbsf).

2.1 Hydrate formation and salinity increase

I initially follow the approach taken by Liu and Flemings [2006] and develop an equilibrium model for hydrate formation, in which volume expansion of hydrate solidification, chemical diffusion, transport of the liquid phase, and latent heat of hydrate crystallization are ignored. In this model, as gas enters the base of the RHSZ, hydrate forms and pore-water salinity increases until free gas coexists with hydrate. With time, this three-phase reaction front propagates toward the seafloor.

The salinity necessary to shift the region of three-phase hydrate stability upward from the base of the RHSZ is calculated using the liquid-hydrate (L+H) and liquid-gas (L+G) methane solubility curves [*Duan et al.*, 1992; *Henry et al.*, 1999] (Fig. 3.1a). If there is no hydrate originally and there is no lateral diffusion of salt, then mass conservation allows me to express hydrate saturation (S_h) with depth (z) as:

$$S_h(z) = 1 - \frac{C_i}{C_{eq}(z)} \tag{3.1}$$

where C_{eq} is the equilibrium salinity at a given depth and C_i is seawater salinity (3.5%) (Fig. 3.1b).

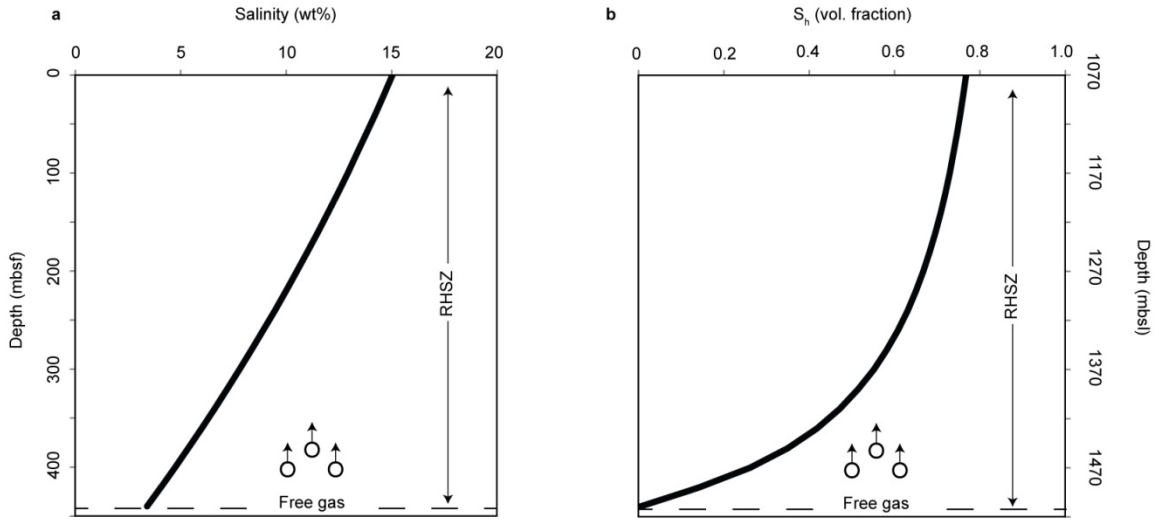

Figure 3.1. Salinity and hydrate saturation associated with steady-state flow for 3-phase hydrate stability.

a, *Plot shows steady-state salinity profile for sustained vertical gas flow. The exclusion of salt during hydrate formation creates a salinity front that propagates toward the seafloor with time.* ***b,*** *Correlative hydrate saturation vs. depth profile for propagating salinity front from part a.*

2.2 Hydrate formation and temperature increase

During hydrate formation, latent heat will be released as hydrate crystallizes [*Cathles and Chen*, 2004; *Liu and Flemings*, 2006]. For the simulated hydrate saturations in Fig. 3.1b, I calculate the resulting temperature change (ΔT):

$$\Delta T = \frac{L\phi\rho_h\Delta S_h}{\rho_b c_b} \tag{3.2}$$

where L is the latent heat of hydrate crystallization (421 kJ kg^{-1}) [*Cathles and Chen*, 2004], ϕ is porosity (0.5), ρ_h is hydrate density (912 kg m^{-3}), and ΔS_h is change in hydrate saturation. Bulk density (ρ_b) and heat capacity (c_b) are expressed as follows:

$$\rho_b = (1-\phi)\rho_s + (\phi S_h \rho_h) + (\phi\rho_w)(1-S_h) \tag{3.3}$$

$$c_b = (1-\phi)c_s + (\phi S_h c_h) + (\phi c_w)(1-S_h) \tag{3.4}$$

where ρ_s and ρ_w are densities of sediment (2650 kg m^{-3}) and water (1035 kg m^{-3}), and c_s, c_w, and c_h are heat capacities of sediment (1381 J K^{-1} kg^{-1}), water (4200 J K^{-1} kg^{-1}), and hydrate (2100 J K^{-1} kg^{-1}). Substituting equations 3.3 and 3.4 into equation 3.2 and integrating equation 3.2, temperature change increases linearly with hydrate saturation (Fig. 3.2b).

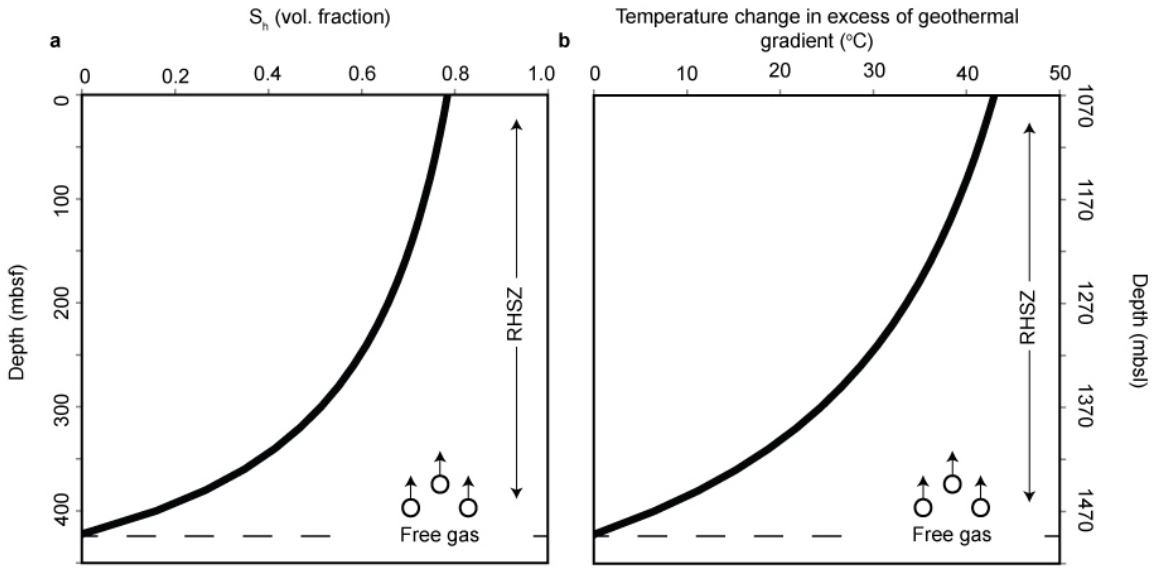

Figure 3.2. Hydrate saturation and temperature change associated with steady-state flow for 3-phase hydrate stability.

a, *Plot shows steady-state hydrate-saturation profile for sustained vertical gas flow. Simulation is the same as in Fig. 3.1b.* ***b,*** *Assuming a perfectly insulated system, figure shows the temperature change resulting from the release of heat during hydrate crystallization for hydrate saturations shown in part a. Temperature change is in excess of temperature change due to the geothermal gradient.*

2.3 Hydrate formation with salinity and temperature increase

Next, I use the L+H and L+G methane solubility curves [*Duan et al.*, 1992; *Henry et al.*, 1999] and equations 3.1, 3.2, and 3.3 to simulate hydrate saturation, salinity, and temperature if heat and salt are simultaneously generated during hydrate formation. In this equilibrium model, significantly less hydrate needs to form to shift the three-phase-stability zone to the seafloor (Fig. 3.3a). This model also results in less significant changes in salinity and temperature as the three-phase reaction front propagates vertically (Fig. 3.3b,c).

The two equilibrium models conceptually explain the enigmatic coexistence of high salinities, elevated temperatures, hydrate formation, and free-gas expulsion at vents. If hydrate formation elevates only salinity as in Liu and Flemings [2006] and temperature follows the geothermal gradient (25 ^{o}C km^{-1}), then hydrate saturations reach ~77% and salinities ~15% at the seafloor (Figs. 3.1, 3.2, 3.4). If latent heat is considered, then hydrate saturations equal ~18% and salinities ~4.3% at the seafloor. Seafloor temperature is ~12.3 ^{o}C which is 7.3 ^{o}C greater than the initial seafloor temperature (5 ^{o}C) (Fig. 3.4). This second model is an end-member model of perfect insulation.

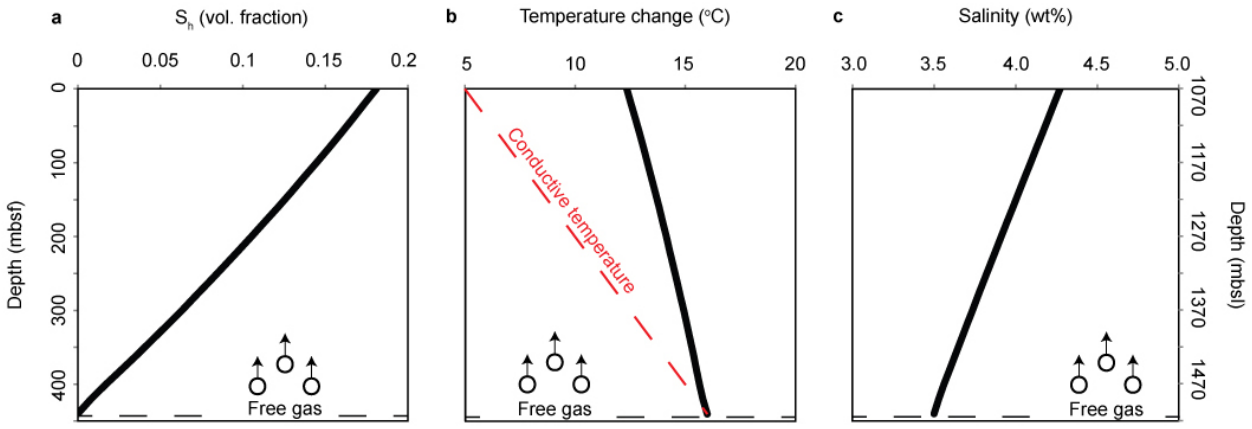

Figure 3.3. Hydrate saturation, temperature, and salinity associated with steady-state flow for 3-phase hydrate stability.

a, *Plot shows steady-state hydrate-saturation profile for sustained vertical gas flow.* ***b,*** *Temperature change resulting from the release of heat during hydrate crystallization for saturations shown in part a.* ***c,*** *Salinities generated via the exclusion of salt for hydrate saturations shown in part a.*

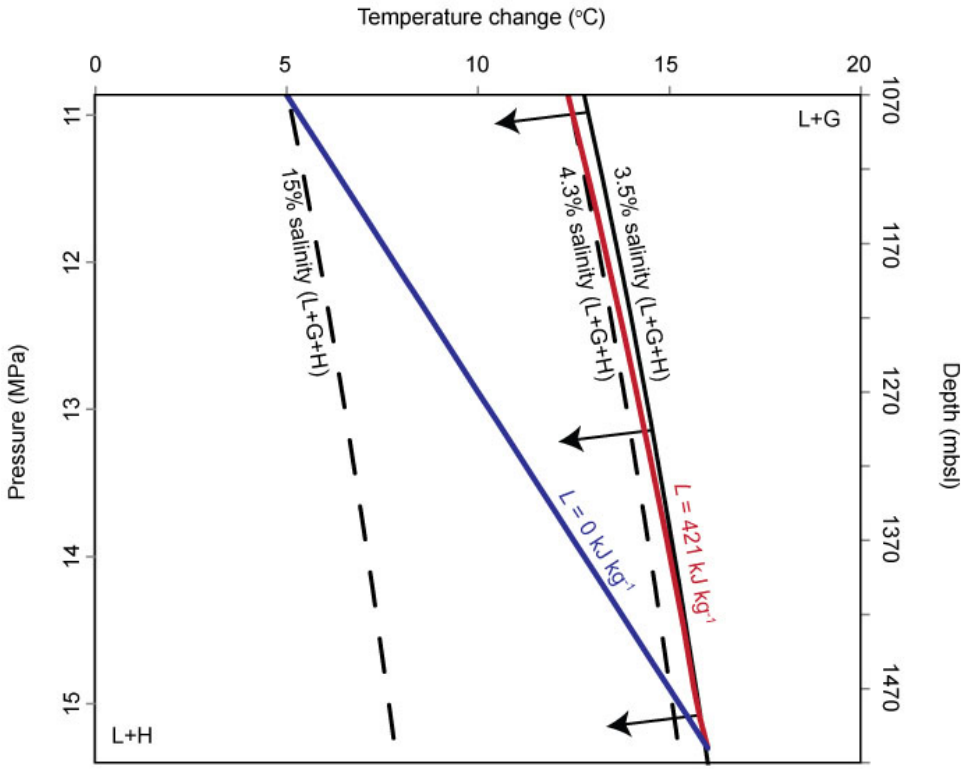

Figure 3.4. Two equilibrium models for venting.

Hydrate stability pressure-temperature phase diagrams for salinities of 3.5% (solid black), 4.3%, (dotted black), and 15% (dotted black). Pressure is converted to depth assuming a hydrostatic pressure gradient (~10.15 MPa km^{-1}). Black arrows show displacement of the phase boundary when salinity increases. If latent heat is not considered (L=0) (Figs. 3.1, 3.2), then salinity increases from 3.5% to 15% and the temperature gradient (blue) follows the geothermal gradient (25 ^{o}C km^{-1}). If it is considered (L=421 kJ kg^{-1}) (Fig. 3.3), then salinity increases from 3.5% to 4.3%, and the temperature gradient (red) is significantly steeper.

3. DYNAMIC MULTIPHASE FLOW MODEL OF HYDRATE FORMATION

I extend the conceptual equilibrium models from part 2 with a one-dimensional multicomponent, multiphase, fluid- and heat-flow model developed by Liu and Flemings [2007]. Again, I model pressure and temperature conditions similar to those at the Ursa vent at lease blocks MC852/853 in the northern GoM. First, I simulate temperature, salinity, free-gas saturations, and hydrate saturations in a hydrate reservoir if latent heat is ignored (L=0). I then simulate each of these variables in a hydrate reservoir where latent heat is accounted for (L=421 kJ kg^{-1}).

I run the two simulations assuming a constant-temperature boundary condition at the seafloor (5 ^{o}C). The temperature at the base of the model column (440 mbsf) is 16 ^{o}C based on a background geothermal gradient of 25 ^{o}C km^{-1} [*Ruppel et al.*, 2005]. I prescribe a constant basal gas flux of 1 kg m^{-2} yr^{-1}. I assume an initial porosity and permeability of 0.5 and 10^{-12} m^{2}, respectively. Salinity is constant (3.5%) throughout the model column at the start of each simulation. Table 3.2 contains the remainder of physical parameters and their sources.

Table 3.2: Physical parameters used for simulations.

Symbol	Parameter	Value [Unit]	Reference
c_h	Heat capacity of hydrate	2100 [J K^{-1} kg^{-1}]	[*Liu and Flemings*, 2007]
C_i	Seawater salinity	3.5 [wt.%]	
c_g	Heat capacity of methane gas	3500 [J K^{-1} kg^{-1}]	[*Liu and Flemings*, 2007]
c_s	Heat capacity of grains	1381 [J K^{-1} kg^{-1}]	[*Liu and Flemings*, 2007]
c_w	Heat capacity of water	4200 [J K^{-1} kg^{-1}]	[*Liu and Flemings*, 2007]
D_m	Diffusion coefficient of methane	10^{-9} [m^2 s^{-1}]	[*Davie and Buffett*, 2001]
D_s	Diffusion coefficient of salt	10^{-9} [m^2 s^{-1}]	[*Davie and Buffett*, 2001]
$dT\ dz^{-1}$	Geothermal gradient	25 [ºC km^{-1}]	[*Ruppel et al.*, 2005; *Winters et al.*, 2007]
g	Gravitational acceleration	9.81 [m s^{-2}]	
k	Permeability in absence of hydrate	10^{-12} [m^2]	[*Liu and Flemings*, 2007]
L	Latent heat of hydrate crystallizations	421 [kJ kg^{-1}]	[*Cathles and Chen*, 2004]
n_g	Corey exponent (gas)	2	[*Bear*, 1972]
n_w	Corey exponent (water)	4	[*Bear*, 1972]
q_g	Basal gas flux	1 [kg m^{-2} yr^{-1}]	This study
q_g	Basal water flux	0 [kg m^{-2} yr^{-1}]	This study
S_{rg}	Irreducible gas saturation	0.02	[*Bear*, 1972]
S_{rw}	Irreducible water saturation	0.1	[*Bear*, 1972]
T_L	Temperature at base of model	16 [ºC]	From T_U and $dT\ dz^{-1}$
T_U	Temperature at seafloor	5 [ºC]	[*Ruppel et al.*, 2005; *Winters et al.*, 2007]
z_o	Depth below sea level	1070 [m]	This study
λ_g	Thermal conductivity of methane	0.03 [W m^{-1} K^{-1}]	[*Sloan*, 1998]
λ_h	Thermal conductivity of hydrate	0.5 [W m^{-1} K^{-1}]	[*Sloan*, 1998]
λ_s	Thermal conductivity of grains	1.6 [W m^{-1} K^{-1}]	[*Class et al.*, 2002]
λ_w	Thermal conductivity of water	0.6 [W m^{-1} K^{-1}]	[*Sloan*, 1998]
μ_g	Dynamic viscosity of gas	P- and T-dependent	[*Class et al.*, 2002]
μ_w	Dynamic viscosity of water	P- and T-dependent	[*Class et al.*, 2002]
ρ_g	Density of methane	P- and T-dependent	[*Duan et al.*, 1992]
ρ_h	Density of hydrate	912 [kg m^{-3}]	[*Sloan*, 1998]
ρ_s	Density of grains	2650 [kg m^{-3}]	
ρ_w	Density of water	T- and salinity-dependent	[*Duan et al.*, 1992]
ϕ	Porosity in absence of hydrate	0.50	

3.1 Case 1: Hydrate solidification model without latent heat

In this simulation, latent heat of hydrate crystallization is ignored. As dissolved gas (1 kg m^{-2} yr^{-1}) fluxes into the model column, its saturation exceeds its solubility, and free gas bubbles form. This free gas migrates into the RHSZ and combines with water to form hydrate. A three-phase zone develops within the RHSZ, in which free gas, dissolved methane, and hydrate coexist (Fig. 3.5). With time, this zone propagates vertically through the RHSZ to the seafloor (Fig. 3.5). After ~22.5 kyr, the three-phase reaction front breaches the seafloor. Within the RHSZ, hydrate saturations increase from 0 to 0.83, and salinity increases from ~3.5% to ~15% just below the seafloor.

Elevated salinities in the RHSZ are created by hydrate formation. As free gas combines with water to form hydrate, salt is excluded, resulting in the generation of saline pore water. Hydrate formation continues until pore water is too saline for further hydrate formation. This process self-generates a three-phase-equilibrium front through the RHSZ. The geothermal gradient (25 ^{o}C km^{-1}) creates colder temperatures closer to the seafloor, therefore pore water needs to be successively saltier at shallower depths in order to create three-phase stability. This results in an upward increase in salinity and hydrate saturation (Fig. 3.5).

Once the reaction front breaches the seafloor (~22.5 kyr), the system reaches a pseudo-steady state. Near the seafloor, salinity diffuses vertically into the overlying water column due to the sharp concentration gradient. This diffusion of salt shifts thermodynamic conditions and allows for further hydrate formation, creating the hydrate spike just below the seafloor (Fig. 3.5). Hydrate saturations at this spike will continue to increase until all the sediment pore space has been filled with hydrate (Fig 3.5). At

deeper depths in the water column, high salinities throughout the RHSZ create a density contrast that causes the hypersaline water to sink (Fig. 3.7). This downward flow of saline water produces salinities greater than the value necessary for three-phase equilibrium at the base of the model (Fig. 3.6a). This downward water flux also causes hydrate to melt at the base of the model, causing hydrate saturations to decrease with time (Fig. 3.6b).

There is significant variability in water and gas flux as a function of depth and time in the system (Fig. 3.7). As the reaction front advances toward the seafloor, an upward water flux develops ahead of the reaction front due to volume expansion during hydrate formation (Fig 3.7a). An upward gas flux is present immediately beneath the reaction front due to the basal gas flux (1 kg m^{-2} yr^{-1}). Once the reaction front breaches the seafloor, free and dissolved methane are continually vented from the RHSZ to the seafloor at a rate slightly > 1 kg m^{-2} yr^{-1} (Fig. 3.7a). This flux is greater than the basal heat flux of 1 kg m^{-2} yr^{-1} because hydrate is melting near the base of the model as a result of the downward flow of dense, saline water (Fig. 3.6b).

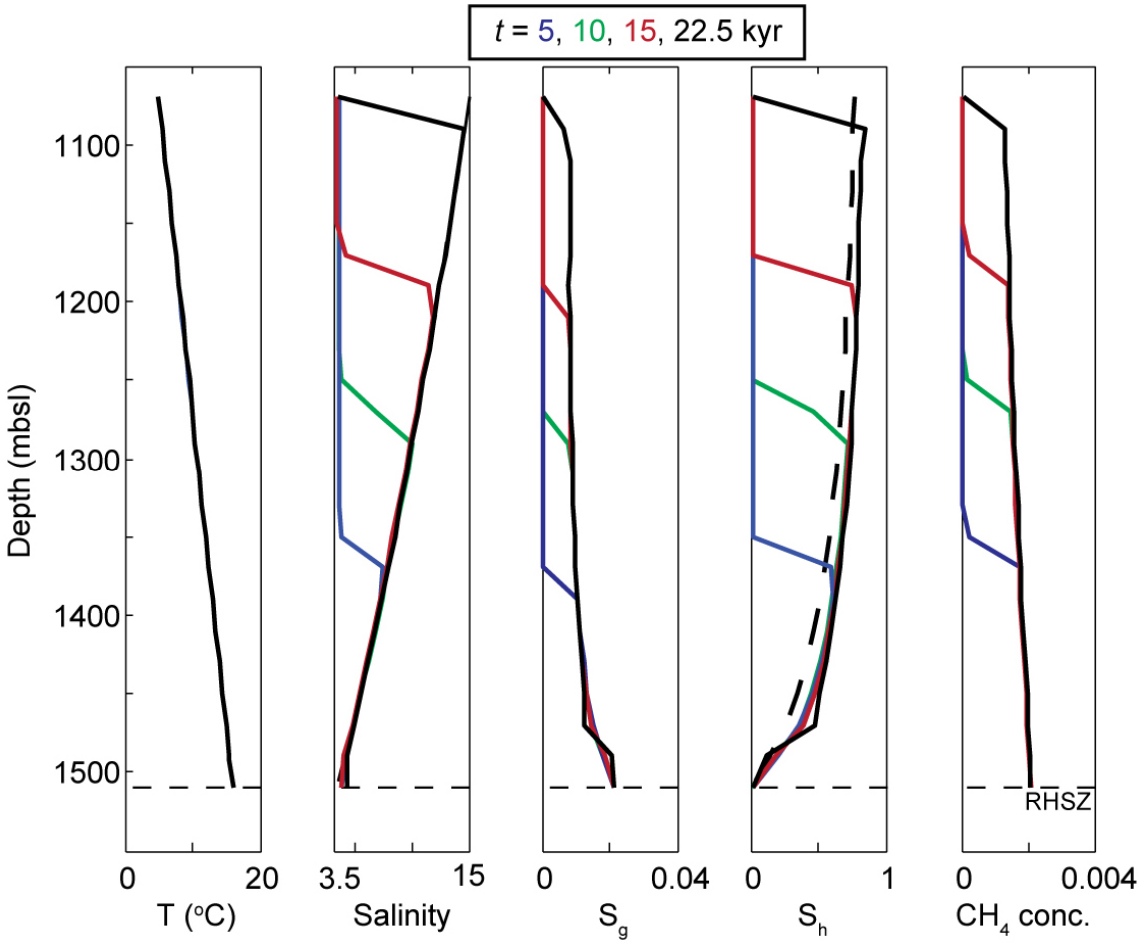

Figure 3.5. Model simulations at different time steps for *L*=0.

Plots showing temporal evolution of temperature (T), salinity (C), gas saturation (S_g), hydrate saturation (S_h), and methane concentration at 5 (blue), 10 (green), 15 (red), and 22.5 (black) kyr. Solid lines are simulated profiles from the dynamic multiphase-flow model, and dotted black lines are profiles from the equilibrium model. At ~22.5 kyr, the reaction front reaches the seafloor. Therafter, free gas vents from the seafloor. The hydrate saturations predicted by the equilibrium model are less than those simulated by the dynamic model. This is because the equilibrium model assumes a closed system, whereas the dynamic model allows for vertical diffusion of salt out of the system.

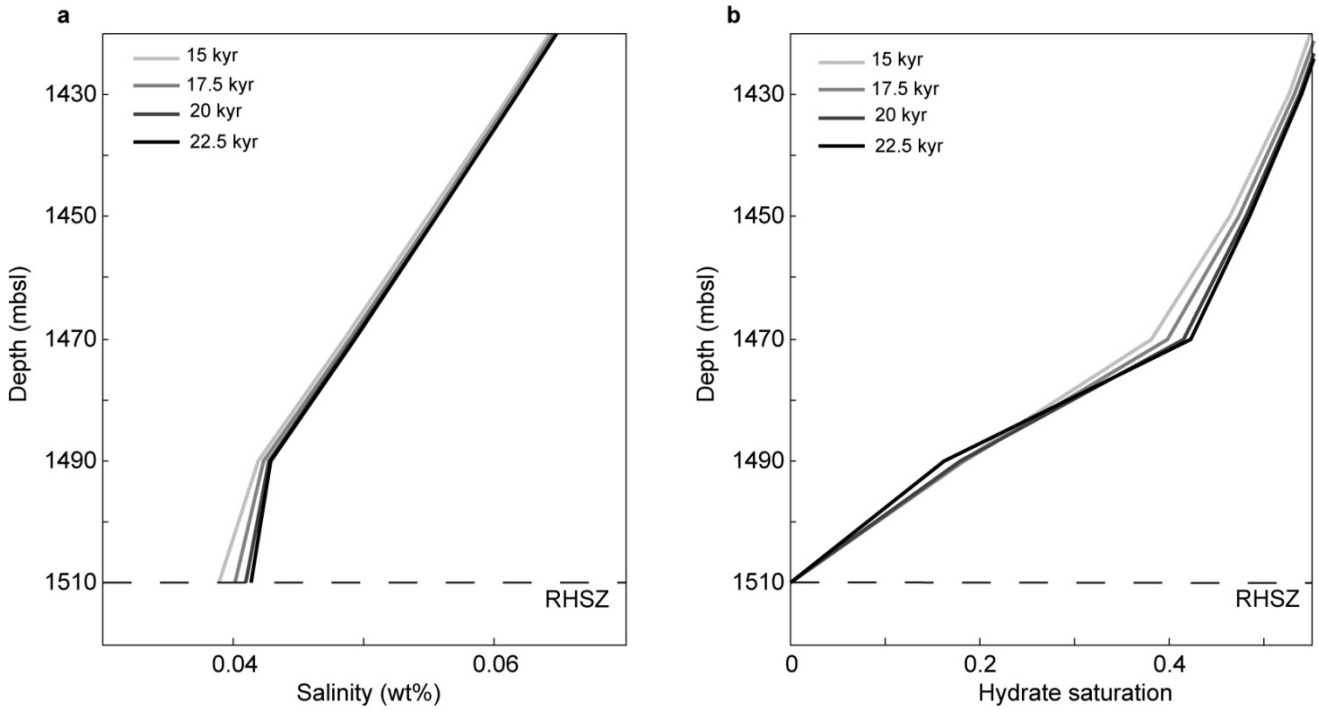

Figure 3.6. Evolution of salinity and hydrate saturation at base of model column after breaching.

a, *Plot showing changes in salinity from 15 kyr (lightest gray) to 22.5 kyr (black). After breaching occurs, salty water sinks from the top of the model column. This process creates salinities that are greater than those required for three-phase equilibrium between 1490 and 1510 mbsl.* ***b,*** *Hydrate saturation decreases with time at the base of the model (1480-1510 mbsl) and increases with time between ~1430-1480 mbsl. Hydrate saturation decreases at the model base due hydrate melting from the downward flow of hypersaline water.*

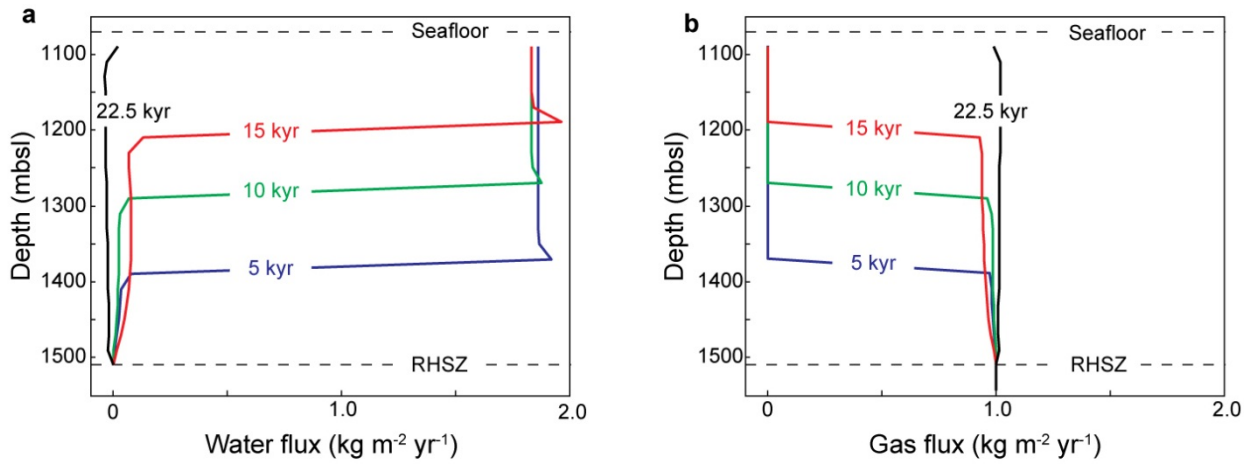

Figure 3.7. Water and gas flux as a function of depth and time for Case 1.

a, b, *Plots show water (a) and gas (b) flux as a function of depth and time. Fluxes vs. depth are correlative with simulations in Fig. 3.5. Flux is calculated using the finite difference code from Liu and Flemings [2007]. Fluxes are calculated every 20 m (block spacing) at block interfaces instead of at block centers. For this reason, flux is not calculated at the seafloor (1070 mbsl) , but 10 meters below seafloor (1080 mbsl). Gas fluxes are cumulative advective and diffusive methane fluxes.*

3.2 Case 2: Hydrate solidification model with latent heat

This simulation is identical to Case 1 except that I consider latent heat of hydrate crystallization. As in Case 1, free gas flows into the RHSZ and combines with water to form hydrate. As hydrate forms, salt is excluded and heat is released, resulting in the generation of a warm, saline brine. With time, hydrate formation develops a zone of three-phase stability within the RHSZ that propagates toward the seafloor (Fig. 3.8). The reaction front breaches the seafloor after ~8.3 kyr, which is significantly faster than Case 1 (~22.5 kyr). This difference in propagation rates is due to the significant amount of heat released (421 kJ kg^{-1}) during hydrate formation.

Initially, the simulated temperatures, salinities, and hydrate saturations from the dynamic model follow those predicted by the equilibrium model (Fig. 3.8). The temperature gradient develops a pronounced concave-down shape, and salinity is elevated slightly above seawater concentrations (Fig. 3.8). But as the reaction front advances further toward the seafloor, a large temperature gradient (~110 ^{o}C km^{-1}) develops between the reaction front and the overlying colder sediments (Fig 3.8). This temperature gradient creates a significant heat flux that draws heat away from the advancing front. As a result, a hydrate and correlative salinity spike develop between 1100 and 1200 mbsl (Fig. 3.8).

The three-phase front breaches the seafloor at ~8.3 kyr. A large salinity gradient develops immediately below the seafloor, and the simulated temperature gradient becomes less concave-down over time (Fig. 3.8). Gas is fluxed from the base of RHSZ to the seafloor (Fig. 3.9). Eventually, the system approaches conditions that are similar to those in Case 1 where latent heat is ignored.

After breaching occurs, the rate of continued hydrate formation is limited by the rate at which salt and heat diffuse out of the system. Salt diffusivity (~10^{-9} m^2 s^{-1}) is significantly smaller than thermal diffusivity (~10^{-6} m^2 s^{-1}), thus salt will be removed from the system more slowly than heat. Therefore, further hydrate formation will be qualified by the rate at which salt diffuses at the seafloor.

For a cell block that is *z*-meters thick and 1-meter wide, the salinity of the cell will be maintained at the equilibrium salinity (C_{eq}), thus the total amount of salt in the cell at time *t* is:

$$zC_{eq}(1 - S_h(t)) \quad (3.5)$$

,

The amount of salt loss by diffusion from this cell from *t* to *t*+*dt* can be calculated using Fick's Law:

$$D_s \frac{Ceq - Ci}{z} dt \quad (3.6)$$

,

where D_s is the diffusion coefficient of salt. At time *t*+*dt*, the total amount of salt in the cell is:

$$zC_{eq}(1 - S_h(t) - \Delta S_h(dt)) \quad (3.7)$$

,

Finally, consider a salt mass balance which equates equation 3.7 with the sum of equations 3.5 and 3.6:

$$zC_{eq}(1-S_h(t)) - D_s \frac{C_{eq}-C_i}{z} dt = zC_{eq}(1-S_h(t)-\Delta S_h(dt)) \quad (3.8)$$

,

which simplifies to:

$$\Delta S_h(dt) = D_s \frac{C_{eq}-C_i}{C_{eq} z^2} dt \quad (3.9)$$

.

For Case 2 of the model with a cell-block thickness of 20 m, the salinity gradient at the seafloor is ~ 0.51 wt% m^{-1} at 12 kyr. The resulting salt flux from the seafloor due to diffusion is 2.55x10^{-9} kg m^{-2} s^{-1} if D_s = 10^{-9} m^2 s^{-1}. The change in hydrate saturation as a function of time based on the flux of salt out of the system is ~1.9x10^{-12} s^{-1} (equation 3.9). The resulting heat flux (q_e) from this change in hydrate saturation can then be calculated using:

$$q_e = \Delta S_h(dt) L \phi \rho_h \quad (3.10)$$

,

where L is latent heat of hydrate crystallization (421 kJ kg^{-1}), ϕ is porosity (0.5), and ρ_h is density of gas hydrate (920 kg m^{-3}). The change in hydrate saturation (ΔS_h, 1.9x10^{-12} s^{-1}) needed to maintain three-phase equilibrium will produce a heat flux of 0.36 mW m^{-2} at the seafloor. By conduction ($q_e = k\ (dt\ dz^{-1})$), a temperature gradient of 0.37 ^oC km^{-1} will result for the average simulated thermal conductivity of 0.97 W m^{-1} K^{-1}. This gradient is ~172x less than the thermal gradient simulated by the model in the first 20 mbsf at 12 kyr (64 ^oC km^{-1}) (Fig. 3.8).

Ultimately, the flux of salt and heat from the seafloor will depend on the grid spacing of the finite-difference code. Smaller grid spacing will drive more rapid diffusion and thus hydrate crystallization near the seafloor. Future work must explore how heat and salt fluxes change as function of the cell size used in the model.

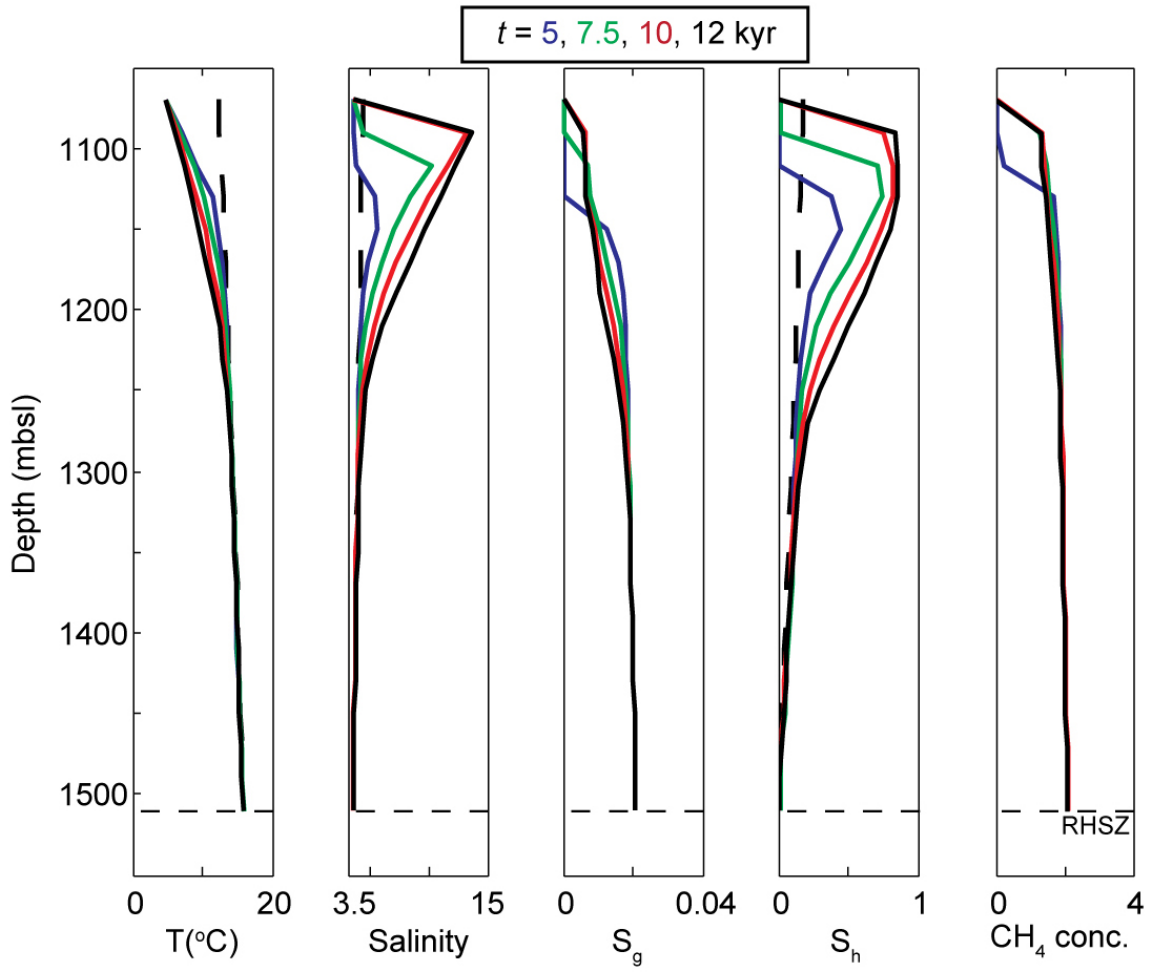

Figure 3.8. Model simulations at different time steps for L=421 kJ kg^{-1}.

Plots showing evolution of temperature (T), salinity (C), gas saturation (S_g), hydrate saturation (S_h), and methane concentration at 5 (blue), 7.5 (green), 10 (red), and 12.5 (black) kyr. Solid lines are simulated profiles from the dynamic multiphase flow model, and dotted black lines are profiles from the equilibrium model. At first, simulated salinities, temperatures, and hydrate saturations from the dynamic model show good agreement with the equilibrium model. But once the reaction front extends closer to the seafloor (<1200 mbsl), the simulated profiles begin to deviate from the equilibrium model. The reaction front breaches the seafloor at ~8.3 kyr.

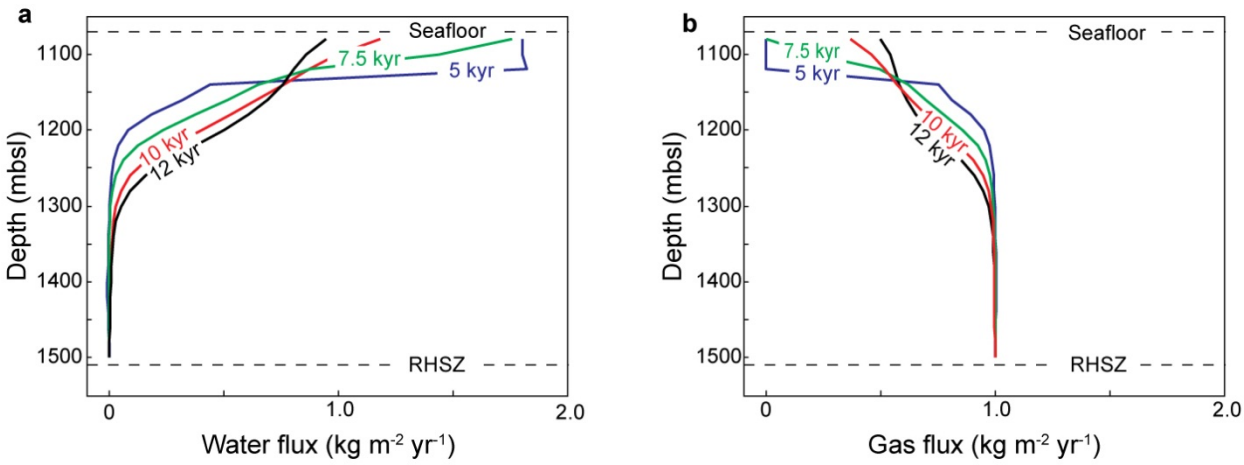

Figure 3.9. Water and gas flux as a function of depth and time for Case 2.

a, b, *Plots show water (a) and gas (b) flux as a function of depth and time for Case 2. Plots are correlative with simulations in figure 3.8.*

4. CONCLUSIONS

I have presented a model that describes how elevated salinities, high temperatures, gas hydrate, and free gas can coexist at deepwater vents such as the Ursa vent in the GoM. The model extends previous work by Liu and Flemings [2006; 2007] by considering the effects of latent heat of hydrate crystallization. The model shows latent heat is initially important in propagating the reaction front to the seafloor. But after ~5 kyr, the temperature front created by hydrate formation is readily removed via conduction. Once the three-phase reaction front breaks through the seafloor, a pseudo-steady state is reached. Further hydrate formation is limited by the rate at which salt diffuses out of the system. This continued hydrate formation sustains a constant flow of salt and heat from the seafloor. The hydrate-solidification model in this chapter simulates a salinity profile that is distinct from that which is simulated by deep advection in Chapter 2. The temperature gradients simulated by hydrate solidification are similar to those predicted by the deep-advection model. Future work should explore hydrate solidification and deep advection as coupled heat- and salt-generating processes at vents.

REFERENCES

Bangs, N. L. B., D. S. Sawyer, and X. Golovchenko (1993), Free gas at the base of the gas hydrate zone in the vicinity of the Chile triple junction, Geology, 21(10), 905-908.

Bear, J. (1972), Dynamics of Fluids in Porous Media, 784 pp., Mineola, N.Y.

Brooks, J. M., H. B. Cox, W. R. Bryant, M. C. Kennicutt Ii, R. G. Mann, and T. J. McDonald (1986), Association of gas hydrates and oil seepage in the Gulf of Mexico, Organic Geochemistry, 10(1–3), 221-234.

Buffett, B. A., and O. Y. Zatsepina (2000), Formation of gas hydrate from dissolved gas in natural porous media, Marine Geology, 164(1–2), 69-77.

Bünz, S., and J. Mienert (2004), Acoustic imaging of gas hydrate and free gas at the Storegga Slide, J. Geophys. Res., 109(B4), B04102.

Cathles, L. M., and D. F. Chen (2004), A compositional kinetic model of hydrate crystallization and dissolution, J. Geophys. Res., 109(B8), B08102.

Class, H., R. Helmig, and P. Bastian (2002), Numerical simulation of non-isothermal multiphase multicomponent processes in porous media.: 1. An efficient solution technique, Advances in Water Resources, 25(5), 533-550.

Clennell, M. B., M. Hovland, J. S. Booth, P. Henry, and W. J. Winters (1999), Formation of natural gas hydrates in marine sediments 1. Conceptual model of gas hydrate growth conditioned by host sediment properties, J. Geophys. Res., 104(B10), 22985-23003.

Daigle, H., and B. Dugan (2010), Effects of multiphase methane supply on hydrate accumulation and fracture generation, Geophys. Res. Lett., 37(20), L20301.

Davie, M. K., and B. A. Buffett (2001), A numerical model for the formation of gas hydrate below the seafloor, J. Geophys. Res., 106(B1), 497-514.

Dickens, G. R. (2003), Rethinking the global carbon cycle with a large, dynamic and microbially mediated gas hydrate capacitor, Earth and Planetary Science Letters, 213(3-4), 169-183.

Duan, Z., N. Møller, J. Greenberg, and J. H. Weare (1992), The prediction of methane solubility in natural waters to high ionic strength from 0 to 250°C and from 0 to 1600 bar, Geochimica et Cosmochimica Acta, 56(4), 1451-1460.

Ellis, M., R. L. Evans, D. Hutchinson, P. Hart, J. Gardner, and R. Hagen (2008), Electromagnetic surveying of seafloor mounds in the northern Gulf of Mexico, Marine and Petroleum Geology, 25(9), 960-968.

Flemings, P. B., X. Liu, and W. J. Winters (2003), Critical pressure and multiphase flow in Blake Ridge gas hydrates, Geology, 31(12), 1057-1060.

Greinert, J., Y. Artemov, V. Egorov, M. De Batist, and D. McGinnis (2006), 1300-m-high rising bubbles from mud volcanoes at 2080m in the Black Sea: Hydroacoustic characteristics and temporal variability, Earth and Planetary Science Letters, 244(1–2), 1-15.

Haeckel, M., E. Suess, K. Wallmann, and D. Rickert (2004), Rising methane gas bubbles form massive hydrate layers at the seafloor, Geochimica et Cosmochimica Acta, 68(21), 4335-4345.

Henry, P., M. Thomas, and M. Ben Clennell (1999), Formation of natural gas hydrates in marine sediments 2. Thermodynamic calculations of stability conditions in porous sediments, J. Geophys. Res., 104(B10), 23005-23022.

Hornbach, M. J., C. Ruppel, D. M. Saffer, C. L. Van Dover, and W. S. Holbrook (2005), Coupled geophysical constraints on heat flow and fluid flux at a salt diapir, Geophys. Res. Lett., 32(24), L24617.

Hyndman, R. D., and E. E. Davis (1992), A Mechanism for the Formation of Methane Hydrate and Seafloor Bottom-Simulating Reflectors by Vertical Fluid Expulsion, J. Geophys. Res., 97(B5), 7025-7041.

Jain, A. K., and R. Juanes (2009), Preferential Mode of gas invasion in sediments: Grain-scale mechanistic model of coupled multiphase fluid flow and sediment mechanics, J. Geophys. Res., 114(B8), B08101.

Judd, A. G. (2003), The global importance and context of methane escape from the seabed, Geo-Marine Letters, 23(3), 147-154.

Kayen, R. E., and H. J. Lee (1991), Pleistocene slope instability of gas hydrate-laden sediment on the Beaufort sea margin, Marine Geotechnology, 10(1-2), 125-141.

Kessler, J. D., W. S. Reeburgh, J. Southon, R. Seifert, W. Michaelis, and S. C. Tyler (2006), Basin-wide estimates of the input of methane from seeps and clathrates to the Black Sea, Earth and Planetary Science Letters, 243(3–4), 366-375.

Kort, E. A., et al. (2012), Atmospheric observations of Arctic Ocean methane emissions up to 82[deg] north, Nature Geosci, 5(5), 318-321.

Kvenvolden, K. A. (1993), Gas hydrates - geological perspective and global change, Rev. Geophys., 31(2), 173-187.

Liu, X., and P. B. Flemings (2006), Passing gas through the hydrate stability zone at southern Hydrate Ridge, offshore Oregon, Earth and Planetary Science Letters, 241(1-2), 211-226.

Liu, X., and P. B. Flemings (2007), Dynamic multiphase flow model of hydrate formation in marine sediments, J. Geophys. Res., 112(B3), B03101.

MacDonald, I. R., W. W. Sager, and M. B. Peccini (2003), Gas hydrate and chemosynthetic biota in mounded bathymetry at mid-slope hydrocarbon seeps: Northern Gulf of Mexico, Marine Geology, 198(1-2), 133-158.

Milkov, A. V., and R. Sassen (2002), Economic geology of offshore gas hydrate accumulations and provinces, Marine and Petroleum Geology, 19(1), 1-11.

Milkov, A. V., G. R. Dickens, G. E. Claypool, Y.-J. Lee, W. S. Borowski, M. E. Torres, W. Xu, H. Tomaru, A. M. Tréhu, and P. Schultheiss (2004), Co-existence of gas hydrate, free gas, and brine within the regional gas hydrate stability zone at Hydrate Ridge (Oregon margin): evidence from prolonged degassing of a pressurized core, Earth and Planetary Science Letters, 222(3-4), 829-843.

Paull, C., W. Ussler, T. Lorenson, W. Winters, and J. Dougherty (2005), Geochemical constraints on the distribution of gas hydrates in the Gulf of Mexico, Geo-Marine Letters, 25(5), 273-280.

Paull, C. K., W. Ussler, W. S. Borowski, and F. N. Spiess (1995), Methane-rich plumes on the Carolina continental rise: Associations with gas hydrates, Geology, 23(1), 89-92.

Reitz, A., M. Haeckel, K. Wallmann, C. Hensen, and K. Heeschen (2007), Origin of salt-enriched pore fluids in the northern Gulf of Mexico, Earth and Planetary Science Letters, 259(3-4), 266-282.

Ruppel, C., G. R. Dickens, D. G. Castellini, W. Gilhooly, and D. Lizarralde (2005), Heat and salt inhibition of gas hydrate formation in the northern Gulf of Mexico, Geophys. Res. Lett., 32(4), L04605.

Shakhova, N., I. Semiletov, A. Salyuk, V. Yusupov, D. Kosmach, and Ö. Gustafsson (2010), Extensive Methane Venting to the Atmosphere from Sediments of the East Siberian Arctic Shelf, Science, 327(5970), 1246-1250.

Sloan, E. D. (1998), Clathrate Hydrates of Natural Gases, 2nd ed., 705 pp., Marcel Dekker, New York.

Smith, A. J., P. B. Flemings, and P. M. Fulton (2011), Observations and models of heat and salt generation in deepwater Gulf of Mexico vents, in Proceedings of the 7th International Conference on Gas Hydrates, edited, p. 12, Edinburgh, Scotland, United Kingdom.

Spieß, V., and N. Fekete (2011), Deep Sea Gas Flares and Associated Gas Hydrate Traps in the Shallow Subseafloor, in 7th International Conference on Gas Hydrates, edited, Edinburgh, Scotland, UK.

Torres, M. E., K. Wallmann, A. M. Tréhu, G. Bohrmann, W. S. Borowski, and H. Tomaru (2004), Gas hydrate growth, methane transport, and chloride enrichment at the southern summit of Hydrate Ridge, Cascadia margin off Oregon, Earth and Planetary Science Letters, 226(1–2), 225-241.

Torres, M. E., J. H. Kim, J. Y. Choi, B. J. Ryu, J. J. Bahk, M. Riedel, T. S. Collett, W. L. Hong, and M. Kastner (2011), Occurence of high salinity fluids associted with massive near-seafloor gas hydrate deposits, in 7th International Conference on Gas Hydrates (ICGH 2011), edited, Edinburgh, Scotland.

Tréhu, A. M., P. B. Flemings, N. L. Bangs, J. Chevallier, E. Gràcia, J. E. Johnson, C. S. Liu, X. Liu, M. Riedel, and M. E. Torres (2004), Feeding methane vents and gas hydrate deposits at south Hydrate Ridge, Geophys. Res. Lett., 31(23), L23310.

Winters, W. J., T. D. Lorenson, and C. K. Paull (2007), Initial Report of the IMAGES VIII/PAGE 127 Gas Hydrate and Paleoclimate Cruise on the RV Marion Dufresne in the Gulf of Mexico, 2-18 July 2002: U.S. Geological Survey Open-File Report 2004-1358, edited.

Wood, W. T., J. F. Gettrust, N. R. Chapman, G. D. Spence, and R. D. Hyndman (2002), Decreased stability of methane hydrates in marine sediments owing to phase-boundary roughness, Nature, 420(6916), 656-660.

Wright, J. F., S. R. Dallimore, F. M. Nixon, and C. Duchesne (2005), In situ stability of gas hydrate in reservoir sediments of the JAPEX/JNOC/GSC et al. Mallik 5L-38 gas hydrate production research wel, Scientific Results from the Mallick 2002 Gas Hydrate Production Research Well Program, Mackenzie Delta, Geol. Surv. Canada, Northwest Territories, Canada.

Xu, W., and C. Ruppel (1999), Predicting the occurrence, distribution, and evolution of methane gas hydrate in porous marine sediments, J. Geophys. Res., 104(B3), 5081-5095.

Yin, P., S. Berné, P. Vagner, B. Loubrieu, and Z. Liu (2003), Mud volcanoes at the shelf margin of the East China Sea, Marine Geology, 194(3-4), 135-149.

Appendix: TRANSPORT AND MULTIPHASE-FLOW MODELS

ABSTRACT

In Chapter 2, I present only analytical solutions to my advection-diffusion and multiphase-flow models. Here I provide a more robust explanation of the physics behind these equations and the assumptions that went into the models. I derive equations 2.2, 2.3, and 2.4 from Chapter 2. Tables A2-A4 contain parameter values for the models, including their references. Table A1 defines the variables that I use.

A1. ASSUMPTIONS

For my models, I make the following simplifying assumptions. (1) The system is in steady state. (2) Heat and salt transport are one-dimensional. (3) Gas and water flow are described by Darcy's Law in a porous media. (4) Methane is the only gas, and water is the only liquid, and neither methane nor water change phase. (5) Methane and water are incompressible, and their heat capacities and viscosities do not change over the flow-path length (i.e. with pressure or temperature). (6) Salt is only transported by water. (7) Permeability and porosity are constant with depth. (8) Pressure drop is negligible in z-direction for material parameters ($P \sim P_o$, but $dP\ dz^{-1} \neq 0$).

A2. SOLUTE-TRANSPORT MODEL

I model chloride anomalies using the solute-transport problem of steady flow between constant-concentration boundaries (assumptions 1, 2). Chloride is transported by chemical diffusion and advection via water (assumption 6):

$$\frac{\partial^2 C}{\partial z^2} - \frac{q_w}{D}\frac{\partial C}{\partial z} = 0 \quad , \tag{A1}$$

where C is Cl^- concentration, z is depth, q_w is water flux, and D is the diffusion coefficient scaled for diffusion in a porous media [*Domenico and Schwartz,* 1990*; Li and*

Table A1: Nomenclature.

Symbol	*Name*	*Dimension**
A	Cross-sectional area of the flow path	L^2
B	Péclet number	Dimensionless
C	Chloride concentration	$M\ L^{-3}$
c_{pw}	Heat capacity (water)	$L^2\ t^{-2}\ T^{-1}$
c_{pg}	Heat capacity (gas)	$L^2\ t^{-2}\ T^{-1}$
D	Diffusion coefficient	$L^2\ t^{-1}$
E_{kg}	Energy density (gas)	$M\ L^{-1}\ t^{-2}$
E_{kw}	Energy density (water)	$M\ L^{-1}\ t^{-2}$
e_z	Energy flux	$M\ t^{-3}$
g	Acceleration due to gravity	$L\ t^{-2}$
$\hat{H}_g$	Specific enthalpy (gas)	$L^2\ t^{-2}$
$\hat{H}_w$	Specific enthalpy (water)	$L^2\ t^{-2}$
k	Permeability	L^2
k_{rg}	Relative permeability of gas	Dimensionless
k_{rw}	Relative permeability of water	Dimensionless
L	Flow-path length	L
P	Pressure	$M\ t^{-2}\ L^{-1}$
P_{cgw}	Gas-water capillary pressure	$M\ L^{-1}\ t^{-2}$
P_g	Gas-phase pressure	$M\ L^{-1}\ t^{-2}$
P_w	Water-phase pressure	$M\ L^{-1}\ t^{-2}$
P^*_w	Overpressure	$M\ L^{-1}\ t^{-2}$
q_c	Heat flux (conduction)	$M\ t^{-3}$
q_g	Gas flux	$L^3\ L^{-2}\ t^{-1}$
Q_g	Volumetric gas flow rate	$L^3\ T^{-1}$
q_w	Water flux	$L^3\ L^{-2}\ t^{-1}$
r	Control volume radius	L
S_{rg}	Irreducible gas saturation	Dimensionless
S_{rw}	Irreducible water saturation	Dimensionless
S_w	Water saturation	Dimensionless
T	Temperature	T
T_L	Temperature at source depth	T
T_U	Temperature at seafloor	T
z	Depth	L
λ	Bulk thermal conductivity	$M\ L\ t^{-3}\ T^{-1}$
μ_g	Gas viscosity	$M\ L^{-1}\ t^{-1}$
μ_w	Water viscosity	$M\ L^{-1}\ t^{-1}$
ρ_g	Gas density	$M\ L^{-3}$
ρ_w	Water density	$M\ L^{-3}$
Φ_g	Gas-phase potential	$M\ L^{-2}\ t^{-2}$

*T=temperature; M=mass; t=time; L=length

Gregory, 1974]. Since I do not have constraints on porosity to 1500 m depth beneath the vent, I adopt the same average scaled diffusion coefficient (2.5×10^{-10} m^2 s^{-1}) as Dugan and Flemings [2000], who modeled Cl^- porewater concentrations in the New Jersey continental slope over a similar length scale. I solve for the Cl^- concentration profile over the flow-path length (L), which I constrain to be 1500 m using Fig. 2.2b.

A2A. Analytical solution for constant-concentration boundary conditions

I apply an analytical solution to equation A1 by choosing constant-concentration boundary conditions over the flow-path length (L). The characteristic equation of equation A1 is:

$$r^2 - \frac{q_w}{D} r = 0 . \tag{A2}$$

The roots of this equation are $r_1 = 0$ and $r_2 = q_w D^{-1}$. The guess equation is:

$$C(z) = C_1 e^{r_1 z} + C_2 e^{r_2 z} . \tag{A3}$$

Substituting r_1 and r_2, equation A3 simplifies to the general solution:

$$C(z) = C_1 + C_2 e^{\frac{q_w}{D} z} . \tag{A4}$$

Choosing constant-concentration boundary conditions at the seafloor (z=0) (C_U) and source depth (z=L) (C_L).

$$C(0) = C_U , \tag{A5}$$

$$C(L) = C_L , \tag{A6}$$

then solving for *C(z)* at *z=0*:

$$C_U = C_1 + C_2 e^{\frac{q_w}{D}0}, \tag{A7}$$

$$C_U = C_1 + C_2, \tag{A8}$$

and solving *C(z)* at *z=L*:

$$C_L = C_1 + C_2 e^{\frac{q_w}{D}L}. \tag{A9}$$

Substituting equation A8 into equation A9 and solving for C_2:

$$C_2 = \frac{C_L - C_U}{e^{\frac{q_w}{D}L} - 1}. \tag{A10}$$

Substituting equation A10 into equation A8 and solving for C_1:

$$C_1 = C_U - \frac{C_L - C_U}{e^{\frac{q_w}{D}L} - 1}. \tag{A11}$$

Substituting equations A10 and A11 into the general solution (equation A1.4):

$$C(z) = C_U - \frac{C_L - C_U}{e^{\frac{q_w}{D}L} - 1} + \left(\frac{C_L - C_U}{e^{\frac{q_w}{D}L} - 1} \right) e^{\frac{q_w}{D}z}, \tag{A12}$$

which simplifies to the final analytical solution (equation 2.1) presented in Chapter 2:

$$C(z) = C_U + \left(C_L - C_U\right) \left(\frac{e^{\frac{q_w z}{D}} - 1}{e^{\frac{q_w L}{D}} - 1} \right). \tag{A13}$$

Table A3 shows parameter values for the solute-transport model.

Table A2: Parameter values for solute-transport model.

Parameter	*Symbol*	*Value [Unit]*	*Reference*
Water flux	q_w	3 [cm yr^{-1}]	This study
Scaled diffusion coefficient	D	2.5 x 10^{-10} [m^2 s^{-1}]	[*Domenico and Schwartz*, 1990; *Dugan and Flemings*, 2000; *Li and Gregory*, 1974]
Cl^- at vent surface (z=0)	C_U	550 [mM]	Concentration in seawater
Cl^- at source depth (z=L)	C_L	2600 [mM]	Approximately highest observed [*Paull et al.*, 2005; *C. Ruppel et al.*, 2005]
Length of the model column	L	1500 [m]	Fig. 2.2b

A3. MULTIPHASE HEAT-TRANSPORT MODEL

I model elevated temperature gradients with steady, vertical groundwater flow between constant-temperature boundaries (assumptions 1, 2). Writing an energy balance for steady-state heating:

$$2\pi r^2 e_z\Big|_z - 2\pi r^2 e_z\Big|_{z+\Delta z} = 0, \tag{A14}$$

where e_z is the total energy flux transferred in/out of the control volume in the z-direction (assumption 2, Fig. A1):

$$e_z = q_g\left(E_{kg} + \rho_g \hat{H}_g\right) + q_w\left(E_{kw} + \rho_w \hat{H}_w\right) + q_c\,, \tag{A15}$$

where the first two terms are heat flow via convection in the gas and water phases, respectively (assumption 4). E_{kg} and E_{kw} are energy densities, and $\hat{H}_g$ and $\hat{H}_w$ are specific enthalpies of gas and water. q_g and q_w are the gas and water fluxes, and ρ_g and ρ_w are the densities of gas and water. The third term is heat flow via conduction and is equivalent to Fourier's Law:

$$q_c = -\lambda \frac{dT}{dz}, \tag{A16}$$

where λ is bulk thermal conductivity and T is temperature. Substituting equations A15 and A16 into equation A14 and dividing by the control volume ($2\pi r^2 \Delta z$) to express in differential form:

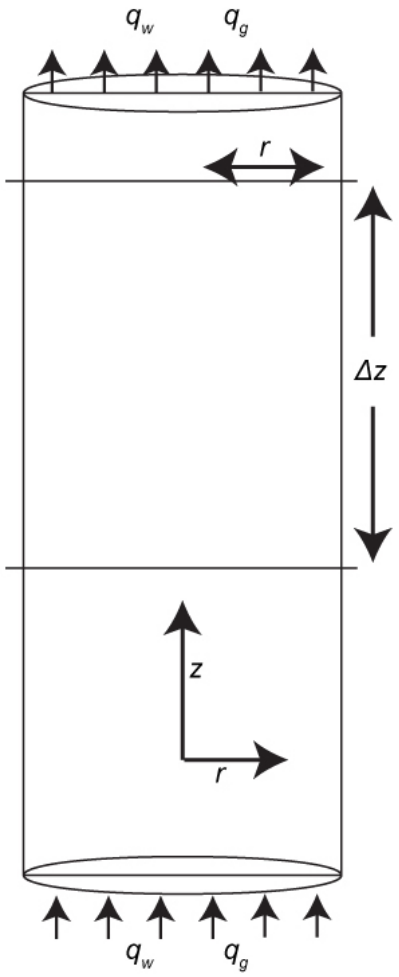

Figure A1. Control volume.

Control volume used for multiphase-heat transport model.

$$\frac{d}{dz}\left(\left(q_g E_{kg} + q_g \rho_g \hat{H}_g\right) + \left(q_w E_{kw} + q_w \rho_w \hat{H}_w\right) - \lambda \frac{dT}{dz}\right) = 0 . \quad \text{(A17)}$$

For an incompressible fluid with constant c_p (assumption 5):

$$\hat{H} = \hat{H}_o + c_p\left(T - T_o\right) + \frac{P - P_o}{\rho} , \quad \text{(A18)}$$

where P is pressure. Substituting equation A18 into equation A17:

$$\frac{d}{dz}\left(\begin{array}{l} q_g E_{kg} + q_g \rho_g \hat{H}_{og} + q_g \rho_g c_{pg}\left(T - T_o\right) + q_g \rho_g \left(P_g - P_{og}\right) + \\ q_w E_{kw} + q_w \rho_w \hat{H}_{ow} + q_w \rho_w c_{pw}\left(T - T_o\right) + q_w \rho_w \left(P_w - P_{ow}\right) - \lambda \frac{dT}{dz} \end{array}\right) = 0 . \quad \text{(A19)}$$

Since q_w and q_g is constant (assumption 1), $E_{kw} = \frac{1}{2}\rho_w {q_w}^2$ is constant; $E_{kg} = \frac{1}{2}\rho_g {q_g}^2$ is constant (assumptions 1, 5); λ is constant (assumption 7); $P \sim P_o$ (assumption 8), then equation A19 is reduced to:

$$\frac{d}{dz}\left(q_g \rho_g c_{pg}\left(T - T_o\right) + q_w \rho_w c_{pw}\left(T - T_o\right)\right) - \lambda \frac{d^2 T}{dz^2} = 0 , \quad \text{(A20)}$$

which simplifies further to:

$$\frac{d^2 T}{dz^2} - \frac{q_w \rho_w c_{pw} + q_g \rho_g c_{pg}}{\lambda} \frac{dT}{dz} = 0 . \quad \text{(A21)}$$

A3A. Analytical solution for constant-temperature boundary conditions

Here, I apply an analytical solution to equation A21 by selecting constant-temperature boundary conditions at the seafloor (T_U) and source depth (T_L) [*Bredehoeft and Papaopulos*, 1965]. The characteristic equation of equation A21 is:

$$r^2 - \frac{q_w \rho_w c_{pw} + q_g \rho_g c_{pg}}{\lambda} r = 0 . \quad \text{(A22)}$$

The roots of this equation are $r_1 = 0$ and $r_2 = (q_w\rho_w c_{pw}+q_g\rho_g c_{pg})\,\lambda^{-1}$. The guess equation is:

$$T(z) = T_1 e^{r_1 z} + T_2 e^{r_2 z}. \tag{A23}$$

Substituting r_1 and r_2, equation A23 simplifies to the general solution:

$$T(z) = T_1 + T_2 e^{\frac{q_w\rho_w c_{pw} + q_g\rho_g c_{pg}}{\lambda} z}. \tag{A24}$$

Choosing constant-temperature boundary conditions at the seafloor (z=0) (T_U) and source depth (z=L) (T_L).

$$T(0) = T_U, \tag{A25}$$

$$T(L) = T_L, \tag{A26}$$

then solving for $T(z)$ at $z=0$:

$$T_U = T_1 + T_2 e^{\frac{q_w\rho_w c_{pw} + q_g\rho_g c_{pg}}{\lambda} 0}, \tag{A27}$$

$$T_U = T_1 + T_2, \tag{A28}$$

and solving $T(z)$ at $z=L$:

$$T_L = T_1 + T_2 e^{\frac{q_w\rho_w c_{pw} + q_g\rho_g c_{pg}}{\lambda} L}. \tag{A29}$$

Substituting equation A28 into equation A29 and solving for T_2:

$$T_2 = \frac{T_L - T_U}{e^{\frac{q_w\rho_w c_{pw} + q_g\rho_g c_{pg}}{\lambda} L} - 1}. \tag{A30}$$

Substituting equation A30 into equation A28 and solving for T_1:

$$T_1 = T_U - \frac{T_L - T_U}{e^{\frac{q_w \rho_w c_{pw} + q_g \rho_g c_{pg}}{\lambda} L} - 1}. \tag{A31}$$

Substituting equations A30 and A31 into the general solution (equation A24):

$$T(z) = T_U - \frac{T_L - T_U}{e^{\frac{q_w \rho_w c_{pw} + q_g \rho_g c_{pg}}{\lambda} L} - 1} + \left(\frac{T_L - T_U}{e^{\frac{q_w \rho_w c_{pw} + q_g \rho_g c_{pg}}{\lambda} L} - 1} \right) e^{\frac{q_w \rho_w c_{pw} + q_g \rho_g c_{pg}}{\lambda} z}, \tag{A32}$$

which simplifies to the final analytical solution (equation 2.2) presented in Chapter 2:

$$T(z) = T_U + (T_L - T_U) \left(\frac{e^{\frac{q_w \rho_w c_{pw} z + q_g \rho_g c_{pg} z}{\lambda}} - 1}{e^{\frac{q_w \rho_w c_{pw} L + q_g \rho_g c_{pg} L}{\lambda}} - 1} \right). \tag{A33}$$

Parameter values for the heat-flow model are in Table A3.

Table A3: Parameter values for multiphase heat-transport model.

Parameter	*Symbol*	*Value [Unit]*	*Reference*
Water flux	q_w	3 [cm yr^{-1}]	This study
Gas flux	q_g	90 [cm yr^{-1}]	This study
Volumetric heat capacity of seawater	$\rho_w c_{pw}$	4.0×10^6 [J m^{-3} K^{-1}]	[*Fofonoff*, 1985]
Volumetric heat capacity of methane (T ~ 5 ºC, P ~ 10 MPa)	$\rho_g c_{pg}$	2.8×10^5 [J m^{-3} K^{-1}]	[*Stetzmann and Wagner*, 1991]
Volumetric heat capacity of oil (T ~ 5 ºC, P ~ 10 MPa)	$\rho_o c_{po}$	1.2×10^6 [J m^{-3} K^{-1}]	Estimated [*Waples and Waples*, 2004]
Bulk thermal conductivity	λ	1.0 [J m^{-1} K^{-1} s^{-1}]	Estimated [*C. Ruppel et al.*, 2005; *Winters et al.*, 2007]
Temperature of bottom water (z=0)	T_U	5 ºC	Estimated [*C. Ruppel et al.*, 2005; *Winters et al.*, 2007]
Temperature at source depth (z=L)	T_L	42.5 ºC	Calculated from T_u, dT/dz, and L
Length of the model column	L	1500 [m]	Fig. 2.2b

A3B. Analytical solution for constant-flux/constant-temperature boundary conditions

In this thesis, I do not use an analytical solution that has a constant heat-flux boundary condition. This solution, however, is widely used in groundwater-flow problems [e.g. *Harris and Chapman*, 1995; *Smith et al.*, 2011], and I present it here. I apply an analytical solution to equation A21 by selecting a constant-temperature boundary condition at the seafloor (T_U) and a constant heat-flux boundary condition at the source depth (Γ_L). I define B as the Péclet number:

$$B = \frac{q_w \rho_w c_{pw} + q_g \rho_g c_{pg}}{\lambda} L \,. \tag{A34}$$

Thus, equation A21 simplifies to:

$$\frac{d^2 T}{dz^2} - \frac{B}{L}\frac{dT}{dz} = 0 \,. \tag{A35}$$

And the characteristic equation is:

$$r^2 - \frac{B}{L} r = 0 \,. \tag{A36}$$

The roots of this equation are $r_1 = 0$ and $r_2 = B\,L^{-1}$. The guess equation is:

$$T(z) = T_1 e^{r_1 z} + T_2 e^{r_2 z} \,. \tag{A37}$$

Substituting r_1 and r_2, equation A37 simplifies to the general solution:

$$T(z) = T_1 + T_2 e^{\frac{Bz}{L}} \,. \tag{A38}$$

Choosing a constant-temperature boundary condition at the seafloor (z=0) (T_U) and constant heat-flux boundary condition at the source depth (z=L) (Γ_L).

$$T(0) = T_U \,, \tag{A39}$$

$$\frac{dT}{dz}(L) = \Gamma_L \,, \tag{A40}$$

then solving the general solution at z=*0*:

$$T_U = T_1 + T_2 \quad . \tag{A41}$$

Taking the derivative of the general solution:

$$\frac{dT}{dz} = \frac{B}{L} T_2 e^{\frac{Bz}{L}} \quad , \tag{A42}$$

and substituting Γ_L for $dT\,dz^{-1}$ and L for z:

$$\Gamma_L = \frac{B}{L} T_2 e^{B} \quad , \tag{A43}$$

I find:

$$T_2 = \frac{\Gamma_L L}{B} e^{-B} \quad . \tag{A44}$$

Substituting equation A44 into equation A41 and solving for T_1.

$$T_1 = T_U - \frac{\Gamma_L L}{B} e^{-B} \quad , \tag{A45}$$

then, substituting equations A44 and A45 into the general solution:

$$T(z) = T_U - \frac{\Gamma_L L}{B} e^{-B} + \frac{\Gamma_L L}{B e^{B}} e^{\frac{B}{L} z} \quad . \tag{A46}$$

Finally, I can simplify to the analytical solution from Harris and Chapman [1995]:

$$T(z) = T_U - \frac{\Gamma_L L}{B} \frac{e^{\frac{B}{L} z} - 1}{e^{B}} \quad . \tag{A47}$$

A4. MULTIPHASE-FLOW MODEL

I begin with a one-dimensional steady-state incompressible flow equation (assumptions 1, 5) for a system that is governed by Darcy's Law (assumption 3):

$$\frac{Q_g}{A} = \frac{kk_{rg}}{\mu_g}\left(\frac{d\Phi_g}{dz}\right), \tag{A48}$$

where Q_g is the volumetric gas flow rate, A is the cross-sectional area of the flow path, k_{rg} is the relative permeability of gas, k is the intrinsic permeability, μ_g is methane viscosity, and Φ_g is gas potential. The gas formation factor is not included in this derivation because I assume gas is incompressible at high pressures (assumption 5), and thus assume it is equal to 1. The gas-phase potential (Φ_g) is defined as:

$$\Phi_g = P_g - \rho_g g z, \tag{A49}$$

where P_g is the gas-phase pressure, ρ_g is the density of gas, g is the acceleration due to gravity, and z is depth. I define the gas-water capillary pressure ($\underline{P_{cgw}}$) for a water-wet system as:

$$P_{cgw} = P_g - P_w, \tag{A50}$$

where P_w is the water-phase pressure. Substituting equation A50 into equation A49, I write the gas phase potential (Φ_g) as:

$$\Phi_g = P_w + P_{cgw} - \rho_g g z, \tag{A51}$$

and the derivative of Φ_g along the flow path becomes:

$$\frac{d\Phi_g}{dz} = \frac{dP_w}{dz} + \frac{dP_{cgw}}{dz} - \rho_g g. \tag{A52}$$

For an incompressible system and constant flow (assumptions 1, 5), gas saturation (S_g) in the fault zone is constant. Therefore P_{cgw} is constant and $dP_{cgw}\, dz^{-1}$ is zero. Equation A52 simplifies to:

$$\frac{d\Phi_g}{dz} = \frac{dP_w}{dz} - \rho_g g \ . \tag{A53}$$

Substituting equation A53 into equation A48, I have a general one-dimensional incompressible flow equation for the flow path:

$$\frac{Q_g}{A} = \frac{kk_{rg}}{\mu_g}\left(\frac{dP_w}{dz} - \rho_g g\right). \tag{A54}$$

In an overpressured system, $\frac{dP_w}{dz} = \frac{dP_w^*}{dz} + \rho_w g$, and I can rewrite equation A54 as:

$$\frac{Q_g}{A} = \frac{kk_{rg}}{\mu_g}\left(\frac{dP_w^*}{dz} + \rho_w g - \rho_g g\right). \tag{A55}$$

Defining $q_g = Q_g A^{-1}$, equation A55 can be rewritten:

$$q_g = \frac{kk_{rg}}{\mu_g}\left(\frac{dP_w^*}{dz} - g\left(\rho_w - \rho_g\right)\right). \tag{A56}$$

The flow of water (q_w) is described by Darcy's Law (assumption 3) and is driven by the overpressure gradient of water:

$$q_w = \frac{kk_{rw}}{\mu_w}\left(\frac{dP_w^*}{dz}\right). \tag{A57}$$

where μ_w is water viscosity, and k_{rw} is the relative permeability of water. Relative permeability (k_{rw}, k_{rg}) describes the effective permeability of a given phase and is related to water saturation (S_w) by using Corey's model [*Bear*, 1972] (Fig. A2):

$$k_{rw} = \left(\frac{S_w - S_{rw}}{1 - S_{rw} - S_{rg}}\right)^4, \tag{A58}$$

$$k_{rg} = \left(1 - \frac{S_w - S_{rw}}{1 - S_{rw} - S_{rg}}\right)^2 \left(1 - \left(\frac{S_w - S_{rw}}{1 - S_{rw} - S_{rg}}\right)^2\right), \tag{A59}$$

where S_{rw} and S_{rg} are irreducible (i.e. minimal) water and gas saturation which are 0.1 and 0.02 for a gas-hydrate system [*Yousif et al.*, 1991]. Substituting equation A58 into equation A57, and equation A59 into equation A56, I get equations 2.3 and 2.4 from Chapter 2. Table A4 lists parameter values for the multiphase-flow model.

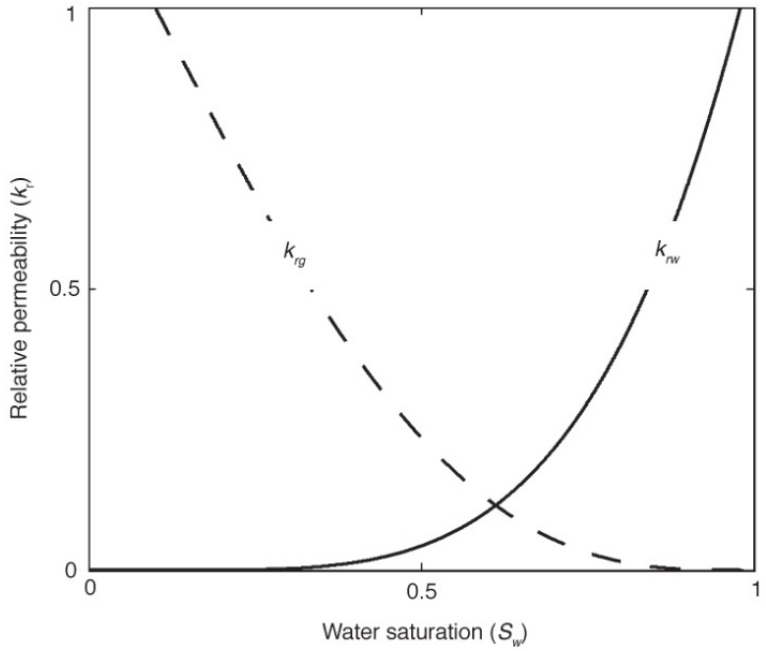

Figure A2. Relative permeability profiles.

Profiles plot the effective permeabilities of gas (dotted) and water (solid) for a given water saturation.

Table A4: Parameter values for multiphase-flow model.

Parameter	*Symbol*	*Value [Unit]*	*Reference*
Water flux	q_w	3 [cm yr^{-1}]	This study
Gas flux	q_g	90 [cm yr^{-1}]	This study
Water viscosity	μ_w	1.1 x 10^{-3} [Pa s]	[*Cox et al.*, 1970]
Methane viscosity	μ_g	1.4 x 10^{-5} [Pa s]	[*Hanley et al.*, 1977]
Water density	ρ_w	1035 [kg m^{-3}]	[*Cox et al.*, 1970]
Methane density	ρ_g	125 [kg m^{-3}]	[*Stetzmann and Wagner*, 1991]
Oil density	ρ_o	600 [kg m^{-3}]	Estimated in this study
Water relative permeability	k_{rw}	Dependent on water saturation (S_w)	[*Bear*, 1972]
Gas relative permeability	k_{rg}	Dependent on water saturation (S_w)	[*Bear*, 1972]
Permeability	k	Fig. 2.4c [m^2]	
Overpressure gradient	$dP^*_w\, dz^{-1}$	Fig. 2.4c [Pa m^{-1}]	
Acceleration due to gravity	g	9.8 [m s^{-2}]	

REFERENCES

Bear, J. (1972), *Dynamics of Fluids in Porous Media*, 784 pp., Mineola, N.Y.

Bredehoeft, J. D., and I. S. Papaopulos (1965), Rates of vertical groundwater movement estimated from the Earth's thermal profile, *Water Resour. Res.*, *1*(2), 325-328.

Cox, R. A., M. J. McCartney, and F. Culkin (1970), The specific gravity/salinity/temperature relationship in natural sea water, *Deep Sea Research and Oceanographic Abstracts*, *17*(4), 679-689.

Domenico, P. A., and F. W. Schwartz (1990), *Physical and chemical hydrogeology*, 824 pp., John Wiley & Sons, New York.

Dugan, B., and P. B. Flemings (2000), Overpressure and Fluid Flow in the New Jersey Continental Slope: Implications for Slope Failure and Cold Seeps, *Science*, *289*(5477), 288-291.

Fofonoff, N. P. (1985), Physical Properties of Seawater: A New Salinity Scale and Equation of State for Seawater, *J. Geophys. Res.*, *90*(C2), 3332-3342.

Hanley, H. J. M., W. M. Haynes, and R. D. McCarty (1977), The viscosity and thermal conductivity coefficients for dense gaseous and liquid methane, *Journal of Physical and Chemical Reference Data*, *6*(2), 597-616.

Harris, R. N., and D. S. Chapman (1995), Climate change on the Colorado Plateau of eastern Utah inferred from borehole temperatures, *Journal of Geophysical Research*, *100*, 6367-6381.

Li, Y.-H., and S. Gregory (1974), Diffusion of ions in sea water and in deep-sea sediments, *Geochimica et Cosmochimica Acta*, *38*(5), 703-714.

Paull, C., W. Ussler, T. Lorenson, W. Winters, and J. Dougherty (2005), Geochemical constraints on the distribution of gas hydrates in the Gulf of Mexico, *Geo-Marine Letters*, *25*(5), 273-280.

Ruppel, C., D. Lizarralde, G. Dickens, and K. Brown (2005), Northern Gulf of Mexico Gas Hydrates (IODP #554): LDEO Site Survey Data Bank Submission Based on NSF-ODP Funded Cruise, edited.

Ruppel, C., G. R. Dickens, D. G. Castellini, W. Gilhooly, and D. Lizarralde (2005), Heat and salt inhibition of gas hydrate formation in the northern Gulf of Mexico, *Geophys. Res. Lett.*, *32*(4), L04605.

Smith, A. J., P. B. Flemings, and P. M. Fulton (2011), Observations and models of heat and salt generation in deepwater Gulf of Mexico vents, in *Proceedings of the 7th International Conference on Gas Hydrates*, edited, p. 12, Edinburgh, Scotland, United Kingdom.

Stetzmann, U., and W. Wagner (1991), A new equation of state and tables of thermodynamic properties for methane covering the range from the melting line to 625 K at pressures up to 1000 MPa, *Journal of Physical and Chemical Reference Data*, *20*, 1061-1151.

Waples, D., and J. Waples (2004), A Review and Evaluation of Specific Heat Capacities of Rocks, Minerals, and Subsurface Fluids. Part 2: Fluids and Porous Rocks, *Natural Resources Research*, *13*(2), 123-130.

Winters, W. J., T. D. Lorenson, and C. K. Paull (2007), Initial Report of the IMAGES VIII/PAGE 127 Gas Hydrate and Paleoclimate Cruise on the RV Marion Dufresne in the Gulf of Mexico, 2-18 July 2002: U.S. Geological Survey Open-File Report 2004-1358, edited.

Yousif, M. H., H. H. Abass, M. S. Selim, and E. D. Sloan (1991), Experimental and Theoretical Investigation of Methane-Gas-Hydrate Dissociation in Porous Media *SPE Reservoir Engineering*, *6*(1), 69-76.

Bibliography

Bangs, N. L. B., D. S. Sawyer, and X. Golovchenko (1993), Free gas at the base of the gas hydrate zone in the vicinity of the Chile triple junction, *Geology*, *21*(10), 905-908.

Bear, J. (1972), *Dynamics of Fluids in Porous Media*, 784 pp., Mineola, N.Y.

Bredehoeft, J. D., and I. S. Papaopulos (1965), Rates of vertical groundwater movement estimated from the Earth's thermal profile, *Water Resour. Res.*, *1*(2), 325-328.

Brooks, J. M., H. B. Cox, W. R. Bryant, M. C. Kennicutt Ii, R. G. Mann, and T. J. McDonald (1986), Association of gas hydrates and oil seepage in the Gulf of Mexico, *Organic Geochemistry*, *10*(1–3), 221-234.

Buffett, B. A., and O. Y. Zatsepina (2000), Formation of gas hydrate from dissolved gas in natural porous media, *Marine Geology*, *164*(1–2), 69-77.

Bünz, S., and J. Mienert (2004), Acoustic imaging of gas hydrate and free gas at the Storegga Slide, *J. Geophys. Res.*, *109*(B4), B04102.

Cathles, L. M., and A. T. Smith (1983), Thermal constraints on the formation of mississippi valley-type lead-zinc deposits and their implications for episodic basin dewatering and deposit genesis, *Economic Geology*, *78*(5), 983-1002.

Cathles, L. M., and D. F. Chen (2004), A compositional kinetic model of hydrate crystallization and dissolution, *J. Geophys. Res.*, *109*(B8), B08102.

Class, H., R. Helmig, and P. Bastian (2002), Numerical simulation of non-isothermal multiphase multicomponent processes in porous media.: 1. An efficient solution technique, *Advances in Water Resources*, *25*(5), 533-550.

Clennell, M. B., M. Hovland, J. S. Booth, P. Henry, and W. J. Winters (1999), Formation of natural gas hydrates in marine sediments 1. Conceptual model of gas hydrate growth conditioned by host sediment properties, *J. Geophys. Res.*, *104*(B10), 22985-23003.

Cox, R. A., M. J. McCartney, and F. Culkin (1970), The specific gravity/salinity/temperature relationship in natural sea water, *Deep Sea Research and Oceanographic Abstracts*, *17*(4), 679-689.

Daigle, H., and B. Dugan (2010), Effects of multiphase methane supply on hydrate accumulation and fracture generation, *Geophys. Res. Lett.*, *37*(20), L20301.

Davie, M. K., and B. A. Buffett (2001), A numerical model for the formation of gas hydrate below the seafloor, *J. Geophys. Res.*, *106*(B1), 497-514.

Dickens, G. R. (2003), Rethinking the global carbon cycle with a large, dynamic and microbially mediated gas hydrate capacitor, *Earth and Planetary Science Letters*, *213*(3-4), 169-183.

Domenico, P. A., and F. W. Schwartz (1990), *Physical and chemical hydrogeology*, 824 pp., John Wiley & Sons, New York.

Duan, Z., N. Møller, J. Greenberg, and J. H. Weare (1992), The prediction of methane solubility in natural waters to high ionic strength from 0 to 250°C and from 0 to 1600 bar, *Geochimica et Cosmochimica Acta*, *56*(4), 1451-1460.

Dugan, B., and P. B. Flemings (2000), Overpressure and Fluid Flow in the New Jersey Continental Slope: Implications for Slope Failure and Cold Seeps, *Science*, *289*(5477), 288-291.

Ellis, M., R. L. Evans, D. Hutchinson, P. Hart, J. Gardner, and R. Hagen (2008), Electromagnetic surveying of seafloor mounds in the northern Gulf of Mexico, *Marine and Petroleum Geology*, *25*(9), 960-968.

Flemings, P. B., X. Liu, and W. J. Winters (2003), Critical pressure and multiphase flow in Blake Ridge gas hydrates, *Geology*, *31*(12), 1057-1060.

Fofonoff, N. P. (1985), Physical Properties of Seawater: A New Salinity Scale and Equation of State for Seawater, *J. Geophys. Res.*, *90*(C2), 3332-3342.

Garcia-Pineda, O., I. R. Macdonald, and D. Villa (2012), Natural Hydrocarbon Seepage Studies in the Gulf of Mexico, edited.

Garcia, O., I. R. MacDonald, B. Zimmer, W. Shedd, and M. Frye (2009), Satellite SAR inventory of Gulf of Mexico oil seeps and shallow gas hydrates, paper presented at EGU General Assembly, Vienna, Austria.

Greinert, J., Y. Artemov, V. Egorov, M. De Batist, and D. McGinnis (2006), 1300-m-high rising bubbles from mud volcanoes at 2080m in the Black Sea: Hydroacoustic characteristics and temporal variability, *Earth and Planetary Science Letters*, *244*(1–2), 1-15.

Haeckel, M., E. Suess, K. Wallmann, and D. Rickert (2004), Rising methane gas bubbles form massive hydrate layers at the seafloor, *Geochimica et Cosmochimica Acta*, *68*(21), 4335-4345.

Hanley, H. J. M., W. M. Haynes, and R. D. McCarty (1977), The viscosity and thermal conductivity coefficients for dense gaseous and liquid methane, *Journal of Physical and Chemical Reference Data*, *6*(2), 597-616.

Hanor, J. S., and J. A. Mercer (2010), Spatial variations in the salinity of pore waters in northern deep water Gulf of Mexico sediments: implications for pathways and mechanisms of solute transport, *Geofluids*, *10*(1-2), 83-93.

Harris, R. N., and D. S. Chapman (1995), Climate change on the Colorado Plateau of eastern Utah inferred from borehole temperatures, *Journal of Geophysical Research*, *100*, 6367-6381.

Hazen, T. C., et al. (2010), Deep-Sea Oil Plume Enriches Indigenous Oil-Degrading Bacteria, *Science*, *330*(6001), 204-208.

Henry, P., M. Thomas, and M. Ben Clennell (1999), Formation of natural gas hydrates in marine sediments 2. Thermodynamic calculations of stability conditions in porous sediments, *J. Geophys. Res.*, *104*(B10), 23005-23022.

Hornafius, J. S., D. Quigley, and B. P. Luyendyk (1999), The world's most spectacular marine hydrocarbon seeps (Coal Oil Point, Santa Barbara Channel, California): Quantification of emissions, *Journal of Geophysical Research*, *104*, 703-711.

Hornbach, M. J., C. Ruppel, and C. L. Van Dover (2007), Three-dimensional structure of fluid conduits sustaining an active deep marine cold seep, *Geophys. Res. Lett.*, *34*(5), L05601.

Hornbach, M. J., C. Ruppel, D. M. Saffer, C. L. Van Dover, and W. S. Holbrook (2005), Coupled geophysical constraints on heat flow and fluid flux at a salt diapir, *Geophys. Res. Lett.*, *32*(24), L24617.

Hu, L., S. A. Yvon-Lewis, J. D. Kessler, and I. R. MacDonald (2012), Methane fluxes to the atmosphere from deepwater hydrocarbon seeps in the northern Gulf of Mexico, *J. Geophys. Res.*, *117*(C1), C01009.

Hubbert, M. K., and D. G. Willis (1972), Mechanics of hydraulic fracturing, *Mem. - Am. Assoc. Pet. Geol.*, *18*, 239-257.

Hyndman, R. D., and E. E. Davis (1992), A Mechanism for the Formation of Methane Hydrate and Seafloor Bottom-Simulating Reflectors by Vertical Fluid Expulsion, *J. Geophys. Res.*, *97*(B5), 7025-7041.

Jain, A. K., and R. Juanes (2009), Preferential Mode of gas invasion in sediments: Grain-scale mechanistic model of coupled multiphase fluid flow and sediment mechanics, *J. Geophys. Res.*, *114*(B8), B08101.

Joye, S. B., et al. (2011), Comment on "A Persistent Oxygen Anomaly Reveals the Fate of Spilled Methane in the Deep Gulf of Mexico", *Science*, *332*(6033), 1033.

Judd, A. G. (2003), The global importance and context of methane escape from the seabed, *Geo-Marine Letters*, *23*(3), 147-154.

Judd, A. G., M. Hovland, L. I. Dimitrov, S. García Gil, and V. Jukes (2002), The geological methane budget at Continental Margins and its influence on climate change, *Geofluids*, *2*(2), 109-126.

Kayen, R. E., and H. J. Lee (1991), Pleistocene slope instability of gas hydrate-laden sediment on the Beaufort sea margin, *Marine Geotechnology*, *10*(1-2), 125-141.

Kessler, J. D., D. L. Valentine, M. C. Redmond, and M. Du (2011a), Response to Comment on "A Persistent Oxygen Anomaly Reveals the Fate of Spilled Methane in the Deep Gulf of Mexico", *Science*, *332*(6033), 1033.

Kessler, J. D., W. S. Reeburgh, J. Southon, R. Seifert, W. Michaelis, and S. C. Tyler (2006), Basin-wide estimates of the input of methane from seeps and clathrates to the Black Sea, *Earth and Planetary Science Letters*, *243*(3–4), 366-375.

Kessler, J. D., et al. (2011b), A Persistent Oxygen Anomaly Reveals the Fate of Spilled Methane in the Deep Gulf of Mexico, *Science*, *331*(6015), 312-315.

Kopf, A. J. (2002), Significance of mud volcanism, *Rev. Geophys.*, *40*(2), 1005.

Kort, E. A., et al. (2012), Atmospheric observations of Arctic Ocean methane emissions up to 82[deg] north, *Nature Geosci*, *5*(5), 318-321.

Kvenvolden, K. A. (1993), Gas hydrates - geological perspective and global change, *Rev. Geophys.*, *31*(2), 173-187.

Leifer, I., and I. R. Macdonald (2003), Dynamics of the gas flux from shallow gas hydrate deposits: interaction between oily hydrate bubbles and the oceanic environment, *Earth and Planetary Science Letters*, *210*(3-4), 411-424.

Leifer, I., and J. Boles (2005), Turbine tent measurements of marine hydrocarbon seeps on subhourly timescales, *Journal of Geophysical Research*, *110*, 1-12.

Li, Y.-H., and S. Gregory (1974), Diffusion of ions in sea water and in deep-sea sediments, *Geochimica et Cosmochimica Acta*, *38*(5), 703-714.

Liu, X., and P. B. Flemings (2006), Passing gas through the hydrate stability zone at southern Hydrate Ridge, offshore Oregon, *Earth and Planetary Science Letters*, *241*(1-2), 211-226.

Liu, X., and P. B. Flemings (2007), Dynamic multiphase flow model of hydrate formation in marine sediments, *J. Geophys. Res.*, *112*(B3), B03101.

MacDonald, I. R., W. W. Sager, and M. B. Peccini (2003), Gas hydrate and chemosynthetic biota in mounded bathymetry at mid-slope hydrocarbon seeps: Northern Gulf of Mexico, *Marine Geology*, *198*(1-2), 133-158.

MacDonald, I. R., D. B. Buthman, W. W. Sager, M. B. Peccini, and N. L. Guinasso (2000), Pulsed oil discharge from a mud volcano, *Geology*, *28*(10), 907-910.

Macdonald, I. R., N. L. Guinasso, Jr., S. G. Ackleson, J. F. Amos, R. Duckworth, R. Sassen, and J. M. Brooks (1993), Natural Oil Slicks in the Gulf of Mexico Visible From Space, *J. Geophys. Res.*, *98*(C9), 16351-16364.

MacDonald, I. R., et al. (2004), Asphpalt volcanism and chemosynthetic life, Campeche Knolls, Gulf of Mexico, *Science*, *304*, 999-1002.

McManus, K. M., and J. S. Hanor (1993), Diagenetic evidence for massive evaporite dissolution, fluid flow, and mass transfer in the Louisiana Gulf Coast, *Geology*, *21*(8), 727-730.

McNutt, M., R. Camilli, G. Guthrie, P. Hsieh, V. Labson, B. Lehr, D. Maclay, A. Ratzel, and M. Sogge (2011), Assessment of Flow Rate Estimates for the Deepwater

Horizon / Macondo Well Oil Spill*Rep.*, National Incident Command, Interagency Solutions Group.

Milkov, A. V., and R. Sassen (2002), Economic geology of offshore gas hydrate accumulations and provinces, *Marine and Petroleum Geology*, *19*(1), 1-11.

Milkov, A. V., R. Sassen, T. V. Apanasovich, and F. G. Dadashev (2003), Global gas flux from mud volcanoes: A significant source of fossil methane in the atmosphere and the ocean, *Geophys. Res. Lett.*, *30*(2), 1037.

Milkov, A. V., G. R. Dickens, G. E. Claypool, Y.-J. Lee, W. S. Borowski, M. E. Torres, W. Xu, H. Tomaru, A. M. Tréhu, and P. Schultheiss (2004), Co-existence of gas hydrate, free gas, and brine within the regional gas hydrate stability zone at Hydrate Ridge (Oregon margin): evidence from prolonged degassing of a pressurized core, *Earth and Planetary Science Letters*, *222*(3-4), 829-843.

Niemann, H., et al. (2006), Novel microbial communities of the Haakon Mosby mud volcano and their role as a methane sink, *Nature*, *443*(7113), 854-858.

NRC (2003), *Oil in the sea III : inputs, fates, and effects* National Academies Press, Washington D.C.

Paull, C., W. Ussler, T. Lorenson, W. Winters, and J. Dougherty (2005), Geochemical constraints on the distribution of gas hydrates in the Gulf of Mexico, *Geo-Marine Letters*, *25*(5), 273-280.

Paull, C., B. Hecker, R. Commeau, R. P. Freeman-Lynde, C. Neumann, W. P. Corso, S. Golubic, J. E. Hook, E. Sikes, and J. Curray (1984), Biological Communities at the Florida Escarpment Resemble Hydrothermal Vent Taxa, *Science*, *226*(4677), 965-967.

Paull, C. K., W. Ussler, W. S. Borowski, and F. N. Spiess (1995), Methane-rich plumes on the Carolina continental rise: Associations with gas hydrates, *Geology*, *23*(1), 89-92.

Reilly, M. J., and P. B. Flemings (2010), Deep pore pressures and seafloor venting in the Auger Basin, Gulf of Mexico, *Basin Res. Basin Research*, *22*(4), 380-397.

Reitz, A., M. Haeckel, K. Wallmann, C. Hensen, and K. Heeschen (2007), Origin of salt-enriched pore fluids in the northern Gulf of Mexico, *Earth and Planetary Science Letters*, *259*(3-4), 266-282.

Ruppel, C., D. Lizarralde, G. Dickens, and K. Brown (2005), Northern Gulf of Mexico Gas Hydrates (IODP #554): LDEO Site Survey Data Bank Submission Based on NSF-ODP Funded Cruise, edited.

Ruppel, C., G. R. Dickens, D. G. Castellini, W. Gilhooly, and D. Lizarralde (2005), Heat and salt inhibition of gas hydrate formation in the northern Gulf of Mexico, *Geophys. Res. Lett.*, *32*(4), L04605.

Sassen, R., S. T. Sweet, A. V. Milkov, D. A. DeFreitas, and M. C. Kennicutt, II (2001), Thermogenic vent gas and gas hydrate in the Gulf of Mexico slope: Is gas hydrate decomposition significant?, *Geology*, *29*(2), 107-110.

Schneider, J. (2011), Compression and permeability behavior of natural mudstones, 302 pp, University of Texas at Austin, Austin.

Shakhova, N., I. Semiletov, A. Salyuk, V. Yusupov, D. Kosmach, and Ö. Gustafsson (2010), Extensive Methane Venting to the Atmosphere from Sediments of the East Siberian Arctic Shelf, *Science*, *327*(5970), 1246-1250.

Sloan, E. D. (1998), *Clathrate Hydrates of Natural Gases*, 2nd ed., 705 pp., Marcel Dekker, New York.

Smith, A. J., P. B. Flemings, and P. M. Fulton (2011), Observations and models of heat and salt generation in deepwater Gulf of Mexico vents, in *Proceedings of the 7th International Conference on Gas Hydrates*, edited, p. 12, Edinburgh, Scotland, United Kingdom.

Solomon, E. A., M. Kastner, I. R. MacDonald, and I. Leifer (2009), Considerable methane fluxes to the atmosphere from hydrocarbon seeps in the Gulf of Mexico, *Nature Geosci*, *2*(8), 561-565.

Spieß, V., and N. Fekete (2011), Deep Sea Gas Flares and Associated Gas Hydrate Traps in the Shallow Subseafloor, in *7th International Conference on Gas Hydrates*, edited, Edinburgh, Scotland, UK.

Stetzmann, U., and W. Wagner (1991), A new equation of state and tables of thermodynamic properties for methane covering the range from the melting line to 625 K at pressures up to 1000 MPa, *Journal of Physical and Chemical Reference Data*, *20*, 1061-1151.

Suess, E., et al. (1999), Gas hydrate destabilization: enhanced dewatering, benthic material turnover and large methane plumes at the Cascadia convergent margin, *Earth and Planetary Science Letters*, *170*(1-2), 1-15.

Torres, M. E., K. Wallmann, A. M. Tréhu, G. Bohrmann, W. S. Borowski, and H. Tomaru (2004), Gas hydrate growth, methane transport, and chloride enrichment at the southern summit of Hydrate Ridge, Cascadia margin off Oregon, *Earth and Planetary Science Letters*, *226*(1–2), 225-241.

Torres, M. E., J. H. Kim, J. Y. Choi, B. J. Ryu, J. J. Bahk, M. Riedel, T. S. Collett, W. L. Hong, and M. Kastner (2011), Occurence of high salinity fluids associted with massive near-seafloor gas hydrate deposits, in *7th International Conference on Gas Hydrates (ICGH 2011)*, edited, Edinburgh, Scotland.

Tréhu, A. M., P. B. Flemings, N. L. Bangs, J. Chevallier, E. Gràcia, J. E. Johnson, C. S. Liu, X. Liu, M. Riedel, and M. E. Torres (2004), Feeding methane vents and gas hydrate deposits at south Hydrate Ridge, *Geophys. Res. Lett.*, *31*(23), L23310.

Valentine, D. L., D. C. Blanton, W. S. Reeburgh, and M. Kastner (2001), Water column methane oxidation adjacent to an area of active hydrate dissociation, Eel river Basin, *Geochimica et Cosmochimica Acta*, *65*(16), 2633-2640.

Valentine, D. L., I. Mezić, S. Maćešić, N. Črnjarić-Žic, S. Ivić, P. J. Hogan, V. A. Fonoberov, and S. Loire (2012), Dynamic autoinoculation and the microbial ecology of a deep water hydrocarbon irruption, *Proceedings of the National Academy of Sciences*.

Waples, D., and J. Waples (2004), A Review and Evaluation of Specific Heat Capacities of Rocks, Minerals, and Subsurface Fluids. Part 2: Fluids and Porous Rocks, *Natural Resources Research*, *13*(2), 123-130.

Wilson, A., and C. Ruppel (2007), Salt tectonics and shallow subseafloor fluid convection: models of coupled fluid-heat-salt transport, *Geofluids*, *7*(4), 377-386.

Winters, W. J., T. D. Lorenson, and C. K. Paull (2007), Initial Report of the IMAGES VIII/PAGE 127 Gas Hydrate and Paleoclimate Cruise on the RV Marion Dufresne in the Gulf of Mexico, 2-18 July 2002: U.S. Geological Survey Open-File Report 2004-1358, edited.

Wood, W. T., J. F. Gettrust, N. R. Chapman, G. D. Spence, and R. D. Hyndman (2002), Decreased stability of methane hydrates in marine sediments owing to phase-boundary roughness, *Nature*, *420*(6916), 656-660.

Wright, J. F., S. R. Dallimore, F. M. Nixon, and C. Duchesne (2005), In situ stability of gas hydrate in reservoir sediments of the JAPEX/JNOC/GSC et al. Mallik 5L-38 gas hydrate production research wel, *Scientific Results from the Mallick 2002 Gas Hydrate Production Research Well Program, Mackenzie Delta, Geol. Surv. Canada, Northwest Territories, Canada*.

Xu, W., and C. Ruppel (1999), Predicting the occurrence, distribution, and evolution of methane gas hydrate in porous marine sediments, *J. Geophys. Res.*, *104*(B3), 5081-5095.

Yin, P., S. Berné, P. Vagner, B. Loubrieu, and Z. Liu (2003), Mud volcanoes at the shelf margin of the East China Sea, *Marine Geology*, *194*(3-4), 135-149.

Yousif, M. H., H. H. Abass, M. S. Selim, and E. D. Sloan (1991), Experimental and Theoretical Investigation of Methane-Gas-Hydrate Dissociation in Porous Media *SPE Reservoir Engineering*, *6*(1), 69-76.